Biochimica et Biophysica Acta 1828 (2013) 1457–1470

Contents lists available at SciVerse ScienceDirect

Biochimica et Biophysica Acta

journal homepage: www.elsevier.com/locate/bbamem

The enhanced membrane interaction and perturbation of a cell penetrating peptide in the presence of anionic lipids: Toward an understanding of its selectivity for cancer cells

Marie-Lise Jobin [a], Pierre Bonnafous [a], Hamza Temsamani [a], François Dole [b], Axelle Grélard [a], Erick J. Dufourc [a], Isabel D. Alves [a,*]

[a] CBMN-UMR 5248 CNRS, Université de Bordeaux, IPB, Allée Geoffroy St. Hilaire, 33600 Pessac, France
[b] CRPP, Centre de Recherche Paul Pascal, 115 Avenue Schweitzer, 33600 Pessac, France

ARTICLE INFO

Article history:
Received 10 December 2012
Received in revised form 29 January 2013
Accepted 15 February 2013
Available online 24 February 2013

Keywords:
Cell penetrating peptide
Peptide/lipid interaction
Lipid model system
Anticancer activity

ABSTRACT

Cell penetrating peptides (CPPs) are usually short, highly cationic peptides that are capable of crossing the cell membrane and transport cargos of varied size and nature in cells by energy- and receptor-independent mechanisms. An additional potential is the newly discovered anti-tumor activity of certain CPPs, including RW16 (RRWRRWWRRWWRRWRR) which is derived from penetratin and is investigated here. The use of CPPs in therapeutics, diagnosis and potential application as anti-tumor agents increases the necessity of understanding their mode of action, a subject yet not totally understood. With this in mind, the membrane interaction and perturbation mechanisms of RW16 with both zwitterionic and anionic lipid model systems (used as representative models of healthy vs tumor cells) were investigated using a large panoply of biophysical techniques. It was shown that RW16 autoassociates and that its oligomerization state highly influences its membrane interaction. Overall a stronger association and perturbation of anionic membranes was observed, especially in the presence of oligomeric peptide, when compared to zwitterionic ones. This might explain, at least in part, the anti-tumor activity and so the selective interaction with cancer cells whose membranes have been shown to be especially anionic. Hydrophobic contacts between the peptide and lipids were also shown to play an important role in the interaction. That probably results from the tryptophan insertion into the fatty acid lipid area following a peptide flip after the first electrostatic recognition. A model is presented that reflects the ensemble of results.

1. Introduction

Cell-penetrating peptides are short peptides that have the ability to translocate into cells in an energy- and receptor-independent manner. CPPs are proven to be vehicles for the intracellular delivery of macromolecules such as oligonucleotides, peptides and proteins, nano-particles and liposomes [1]. Therefore these molecules present a great potential in therapeutics and diagnosis. Indeed, the number of applications using CPPs is quickly increasing, with so far more than 300 studies from in vitro to in vivo using CPP-based strategies [2–6]. Since their discovery in the 1990s an important number of research groups have focused in the understanding of their mode of action with the final attempt of improving their internalization and specificity. It is now mostly agreed that their uptake occurs through both endocytotic and non-endocytotic pathways but the molecular requirements for an efficient internalization are not fully understood [7]. It appears that their uptake ability depends on their amino acid sequence and spacing [8]. Despite their uptake being endocytotic or not, the first barrier that these peptides encounter is the plasma membrane which prevents direct translocation of macromolecules.

Herein, we have focused in the understanding of the membrane interaction and perturbation by a CPP derived from penetratin SAR (structure–activity relationship) studies. The peptide is RW16 (RRWRRWWRRWWRRWRR), a 16 residue amphipathic peptide shown to be a good CPP [9]. Moreover this peptide was reported to possess anti-tumor activity, namely, to decrease the mobility and proliferation of cancer cells (EF cells), this without being cytotoxic (up to 20 μM; in both NIH 3T3 and EF cells) [10]. The mechanism of action of this peptide is not well understood. Lamaziere et al. have shown that RW16 induced GUVs (Giant Unilamellar Vesicles) adhesion and vesicle aggregation for certain lipid compositions. Aside from these liposome modifications

Abbreviations: AMP, Anti-microbial peptide; APA, Amino pentanoic acid; CD, Circular dichroism; CHO, Chinese hamster ovary; CPP, Cell-penetrating peptide; DLS, Dynamic Light Scattering; DMPC, Dimyristoyl phosphatidylcholine; DMPG, Dimyristoyl phosphatidylglycerol; DOPC, Dioleoyl phosphatidylcholine; DOPE, Dioleoyl phosphatidylethanolamine; DOPG, Dioleoyl phosphatidylglycerol; DOPS, Dioleoyl phosphatidylserine; DPPC, Dipalmitoyl phosphatidylcholine; DSC, Differential Scanning Calorimetry; GUV, Giant Unilamellar Vesicle; ITC, Isothermal Titration Calorimetry; LUV, Large unilamellar vesicle; MIC, Minimal inhibitory concentration; MLV, Multilamellar vesicle; PC, Phosphatidylcholine; PE, Phosphatidylethanolamine; PG, Phosphatidylglycerol; PS, Phosphatidylserine; SAR, Structure–activity relationship

* Corresponding author. Tel.: +33 5 40 00 68 49.
E-mail address: i.alves@cbmn.u-bordeaux.fr (I.D. Alves).

0005-2736/$ – see front matter © 2013 Elsevier B.V. All rights reserved.
http://dx.doi.org/10.1016/j.bbamem.2013.02.008

they have found that RW16 induced calcein leakage without being lethal to the cells [11]. It is interesting to notice that recent studies have shown that some CPPs preferentially accumulate in cancer cells [12–14]. This selectivity toward cancer vs healthy cells might be directly correlated with the richness in anionic components in their cell membranes. Indeed several studies indicated that cancer cell membranes overexpress certain proteoglycans such as glypicans and syndecans which are implicated in several aspects of tumorigenesis such as cell adhesion, growth and motility [15–18]. Additionally, when cells become apoptotic their transmembrane asymmetry is strongly perturbed with an increase in the levels of phosphatidylserine (PS) in the outer membrane leaflet, of up to 9% [19]. These components in the cancer cell membranes render them additionally anionic relative to healthy cell membranes which can be favorable for the interaction with cationic molecules such as CPPs.

In the present study the structural characterization and interaction mechanism of RW16 with different membrane models (composed of zwitterionic and/or anionic lipids) was performed. The zwitterionic lipid system was employed as a mimic of the outer leaflet of a healthy eukaryotic cell and the anionic system to model the enhanced anionic character of apoptotic cells. The interaction, affinity, perturbation of the lipid model systems upon RW16 interaction as well as the structural changes occurring in the peptide upon this interaction was investigated. Studies were performed using several biophysical techniques and lipid model systems to mimic healthy and cancer cell membranes. CPPs and antimicrobial peptides share common features namely their cationic nature [20] and in the particular case of RW16 the amphipathicity. Additionally several cell penetrating peptides have been reported to possess antimicrobial activity, including penetratin and its analogues [21–25]. Therefore the antimicrobial activities of RW16 were investigated against *Escherichia coli*, *Staphylococcus aureus* and *Klebsiella pneumoniae*. Furthermore efficient antimicrobial peptides have also been shown to possess anticancer activity [26–28].

The analysis of the results obtained was complicated by the fact that RW16 alone autoassociates at increasing peptide concentrations, a property arising from its amphipathic character. Overall the studies indicate an enhanced interaction and perturbation of RW16 with anionic vs zwitterionic lipids which is specially marked when the peptide is in its oligomerized form. While this would indicate that electrostatic interactions are important in the P/L interaction, which is rather expected, the studies show that important hydrophobic interactions take place. Such interactions can be explained by a peptide flip, following the initial electrostatic contacts, probably around the Arg with the insertion of Trp residues in the fatty acid chain core. A model is proposed to explain the markedly distinct behavior of RW16 in interaction with anionic vs zwitterionic lipids that also takes into account the peptide oligomerization state. This preferential interaction and perturbation in membranes enriched in anionic components may explain the reported anti-tumor activity of this peptide and CPPs in general.

2. Materials & methods

2.1. Materials

All lipids were purchased from Avanti Polar Lipids (Alabaster, AL). The calcein was obtained from Sigma. Biot(O_2)-Apa-RW16-NH_2 (RRWRRWWRRWWRRWRR) synthesis and purification was performed using Boc solid phase strategy. The bacterial strains were kindly provided by the laboratory of Pierre Nicolas.

2.2. Antimicrobial activity

Gram-positive eubacteria (*S. aureus*) and Gram-negative eubacteria (*E. coli 363* and *K. pneumoniae*) were cultured as described previously [29]. The minimal inhibitory concentrations (MICs) of peptides were determined in 96-well microtitration plates by growing the bacteria in the presence of 2-fold serial dilutions of peptide. Aliquots (10 μL) of each serial dilution were incubated for 16 h at 37 °C with 100 μL of a suspension of a midlogarithmic phase culture of bacteria, at a starting absorbance $A_{630} = 0.01$ in Poor-Broth nutrient medium (1% bactotryptone and 0.5% NaCl, w/v) (peptide final concentrations ranged from 0.1 to 100 μM). Inhibition of growth was assayed by measuring the absorbance at 630 nm. The MIC was defined as the lowest concentration of peptide that inhibited the growth of about 99% of the cells. Bacteria that was incubated with the peptide corresponding to the MIC was plated out on solid culture medium containing 1% noble agar to distinguish between lytic and non-lytic effects. The peptide was considered to be lytic if after overnight incubation with the peptide (at the MIC concentration) the bacteria development was inhibited and non-lytic when the bacteria was able to re-grow upon peptide incubation. All assays were performed in triplicate plus positive controls without the peptide and negative controls with 0.7% formaldehyde.

2.3. Preparation of liposomes

All liposomes were prepared by initially dissolving the appropriate amount of phospholipids, to obtain the desired concentration, in chloroform and methanol (2/1 v/v) to ensure the complete mixing of the components. A lipid film was then formed by removing the solvent using a stream of N_2 (g) followed by 3 h vacuum. To form MLVs, the dried lipids were dispersed in buffer (either Tris 10 mM, 150 mM NaCl, 2 mM EDTA pH 7.4 or phosphate 10 mM, NaCl 150 mM, EDTA 2 mM pH 7.4 buffer depending on the technique used) and thorough vortexed. To form LUVs, the MLV dispersion was run through five freeze/thawing cycles and passed through a mini-extruder equipped with two stacked 0.1 μm polycarbonate filters (Avanti, Alabaster, AL).

2.4. Turbidity

Turbidity of LUVs was followed by measuring the absorbance at 436 nm upon addition of increasing peptide concentration (P/L ratios of 1/100, 1/50, 1/25, 1/10 were used). The measurements were acquired on a Jasco V-630 spectrometer at room temperature (~22 °C).

2.5. Dynamic Light Scattering (DLS)

DLS measurements were performed using an ALV laser goniometer, equipped with a 22 mW HeNe linearly polarized laser operating at 632.8 nm and an ALV-5000/EPP multiple τ digital correlator with 125 ns initial sampling time. Measurements were performed at a scattering angle of 90° and the intensity correlation functions were analyzed using the software provided by the company, to give the hydrodynamic radius (Rh) of the scattering particles. All measurements were performed at room temperature in phosphate buffer. To get an insight into the influence of RW16 on LUVs integrity, 100 μL of a 1 mg/mL LUV solution was analyzed by DLS, followed by addition of a small volume of RW16 (1 mM) to the LUV suspension to the desired P/L ratio (1/100, 1/50, 1/25, 1/10) and particle size again analyzed, immediately. The same measurements were performed in the absence of LUVs to determine whether the peptide auto-aggregates.

2.6. Tryptophan fluorescence

Small volumes of LUV suspensions (1 mM) were successively added to the peptide solution (0.5 μM) to obtain different P/L ratios: 1/10, 1/25, 1/50 and 1/100. After 2 min incubation, fluorescence spectra were recorded using an excitation wavelength (λ_{exc}) of 278 nm (5 nm bandwidth) and emission wavelength (λ_{em}) in the interval from 300 nm to 500 nm (10 nm bandwidth). The scan speed was 200 nm/min and the spectra were averaged over 10 accumulations. Fluorescence measurements were made on a Perkin Elmer LS55 spectrometer (Buckinghamshire, UK). The blue shift was plotted against the lipid concentration and fitted using a hyperbolic function being

able to provide the concentration of lipids at which the half-shift of the Trp emission spectrum was observed.

2.7. Calcein leakage

Calcein-containing LUVs were made using the same protocol used to make regular LUVs, except for the hydration step made with Tris buffer of the lipid films, which contained 70 mM calcein [30]. Free calcein was separated from the calcein-containing LUVs using size exclusion column chromatography (Sephadex G-75) with Tris as elution buffer. The concentration of lipids was estimated using Rouser protocol [31]. For the assay, the lipid concentration was set at 1 μM and peptide concentration was allowed to vary from 1 nM to 500 nM (P/L ratio of 1/1000 to 1/2 respectively). All measurements were performed with a Perkin Elmer LS55 spectrometer (Buckinghamshire, UK). Data were collected every 1 s at room temperature using a λ_{exc} at 485 nm and λ_{em} at 515 nm with an emission and excitation slit of 2.5 nm in a cuvette of 2 mL.

The fluorescence from calcein at 70 mM concentration was low due to self-quenching, but increased considerably upon dilution. The fluorescence intensity at the equilibrium was measured after 2.5 h. At the end of the assay, complete leakage of LUVs was achieved by adding 100 μL of 10% Triton X-100 solution dissolving the lipid membrane without interfering with the fluorescence signal. The percentage of calcein release was calculated according to the following equation:

$$\%\text{Calcein leakage} = (\text{Ft}-\text{Fo})/(\text{Ff}-\text{Fo})*100 \quad (1)$$

where the percent of calcein leakage is the fraction of dye released (normalized membrane leakage), Ft is the measured fluorescence intensity at time t, and Fo and Ff are respectively the fluorescence intensities at times t = 0, and after final addition of Triton X-100, respectively. A dilution correction was applied on the fluorescence intensity after injection of the Triton X-100. Each experiment was repeated three times.

2.8. ^{31}P Nuclear Magnetic Resonance (^{31}P NMR)

MLVs were prepared as described in Section 2.3 at a concentration of 150 mg/mL in D_2O/H_2O (90:10) and NMR acquisition was performed in a rotor of 100 μL. The peptide was added as a powder to the liposomes to obtain a P/L ratio of 1/100 and then thoroughly vortexed to ensure sample equilibrium. NMR experiments were carried out on a Bruker Advance DPX 400 NB spectrometer by the mean of a QNP-Probe ($^{1}H/^{31}P-^{13}C-^{19}F$). ^{31}P NMR spectra were acquired at 161.97 MHz, using a phase-cycled Hahn-echo pulse sequence with gated broadband proton decoupling. Typical acquisition parameters were as follows: spectral window of 50 kHz, π/2 pulse widths of 14 μs, interpulse delays of 50 μs, a recycle delay of 5 s, 128 scans were recorded and a scanning of temperature from 2 to 20 °C was applied. A line broadening of 50 Hz and baseline correction was usually applied prior to Fourier transformation. The amount of each phase (lamellar, hexagonal and isotropic phases) was determined by simulation of the experimental spectrum [32] (T. Pott and E.J. Dufourc, unpublished data).

2.9. Circular dichroism (CD)

CD data was recorded on a Jasco J-815 CD spectrophotometer with a 1 mm path length. Far-UV spectra were recorded from 180 to 270 nm with a 0.5 nm step resolution and a 2 nm bandwidth at 37 °C. The scan speed was 50 nm/min (0.5 s response time), and the spectra were averaged over 8 scans. CD spectra were collected for samples of RW16 in phosphate buffer with and without liposomes at different P/L ratios (1/100, 1/50, 1/25, 1/10). For each sample, the background (buffer) was automatically subtracted from the signal. Spectra were smoothed using a Savitzky–Golay smoothing filter. Spectra were deconvoluted using the software CD Friend previously developed in our laboratory (S. Buchoux, unpublished).

2.10. Plasmon Waveguide Resonance (PWR)

PWR spectra are produced by resonance excitation of conduction electron oscillations (plasmons) by light from a polarized CW laser (He–Ne; wavelength of 632.8 and 543.5 nm) incident on the back surface of a thin metal film (Ag), deposited on a glass prism and coated with a layer of SiO_2. Experiments were performed on a beta PWR instrument from Proterion Corp. (Piscataway, NJ) that had a spectral angular resolution of 1 mdeg. PWR spectra, corresponding to plots of reflected light intensity versus incident angle, can be excited with light whose electric vector is either parallel (*s*-polarization) or perpendicular (*p*-polarization) to the plane of the resonator surface.

The sample to be analyzed (a lipid bilayer membrane) was immobilized on the resonator surface and placed in contact with an aqueous medium, into which drugs can be introduced. The self-assembled lipid bilayers were formed using a solution (in butanol/squalene 95/5 v/v) of 10 mg/mL of lipids. The method used to make the lipid bilayers is based on the procedure by Mueller and Rudin to make black lipid membranes across a small hole in a Teflon block [33]. To accomplish this, a small amount (~2.5 μL) of lipid solution was injected into the orifice in a Teflon block separating the silica surface of the PWR resonator from the aqueous phase. Spontaneous bilayer formation was initiated when the sample compartment was filled with aqueous buffer solution. The molecules (such as lipids and drugs) deposited onto the surface plasmon resonator change the resonance characteristics of the plasmon formation and can thereby be detected and characterized (for more details see [34]). The peptide was injected into the cell sample compartment containing the lipid membrane in an incremental fashion. The amount of lipid bound drug is associated with the resonance shift observed by PWR, the total amount being the amount of drug added to the chamber. Since the PWR is only sensitive to the optical properties of material that is deposited on the resonator surface, there is no interference from the material that is in the bulk solution. Moreover, the amount of bound material is much smaller than the total amount of peptide present in the bulk solution, and it is assumed that the bulk material is able to freely diffuse and equilibrate with the membrane. Data were fitted (GraphPad Prism) through the following hyperbolic function that describes the binding of a ligand to a receptor, providing the dissociation constants: $Y = (B\text{max } X)/(K\text{d} + X)$. *B*max represents the maximum concentration bound, and *K*d is the concentration of ligand required to reach half-maximal binding [35]. It should be noted that since concomitantly with the binding process other processes, such as membrane reorganization and solvation occur, the dissociation constants correspond to apparent dissociation constants. Graphical analysis allows one to obtain information about changes in the mass density, structural asymmetry, and molecular orientation induced by bimolecular interactions occurring at the resonator surface. By plotting the spectral changes observed in a (*s*, *p*) coordinate system where mass (Δ_m) and anisotropy (Δ_{str}) axes are represented based on the PWR sensitivity factor, the contribution of mass and structural changes can be obtained [36,37]. Each point in the mass and anisotropy axis can be expressed by changes in the original coordinates (Δp and Δs) by the following equations:

$$\Delta_m = \left[(\Delta s)_m^2 + (\Delta p)_m^2\right]^{1/2} \quad (2)$$

$$\Delta_{str} = \left[(\Delta s)_{str}^2 + (\Delta p)_{str}^2\right]^{1/2} \quad (3)$$

The sensitivity factor (*Sf*), a measure of the sensitivity of the instrument for the *s*-polarization relative to *p*-polarization ($Sf = \Delta s/\Delta p$), necessary to determine the mass and anisotropy axes has been determined, for the prism used in those experiments, to be 0.74 [38].

2.11. Differential Scanning Calorimetry (DSC)

Microcalorimetry experiments were performed with a Nano DSC-II microcalorimeter (CSC) driven by a DSC-run software. The peptide was gradually added to the same sample of lipid MLVs to obtain peptide/lipid molar ratios of 1/100, 1/50 and 1/25. The lipid concentration was 1 mg/mL (ca. 1.45 mM), except for: DMPG/DPPC where the concentration was 4 mg/mL (ca. 5.66 mM), DMPC/Chol and DMPG/Chol where the concentration was 6 mg/mL (ca. 8.9 and 9.05 mM respectively). For each peptide concentration, a minimum of four heating and four cooling scans were performed so that equilibrium is reached. A scan rate of 1 °C/min was used and there was a delay of 10 min between sequential scans in a series to allow thermal equilibration. Data analysis was performed by the fitting program CPCALC provided by CSC and using the Software Origin for the deconvolution.

2.12. Isothermal Titration Calorimetry (ITC)

ITC experiments were performed on a Microcal ITC200 at different temperatures between 15 and 40 °C. To avoid air bubbles, peptide and LUV solutions were degassed under vacuum before use. Titrations were performed by injecting 2.5 μL aliquots of LUVs (lipid concentration 12.6 mM in a syringe of 40 μL) into the calorimeter cell of 200 μL containing the peptide solution (peptide concentration 0.1 mM), with 10 min waiting between injections. A blank was performed where the LUVs were titrated into the same buffer used for the above experiments (Tris buffer). Data analysis was performed using the program Origin 7.0 microCal. All curves were fit using a nonlinear least-squares "One Set of Sites" (1:1 interactions) model.

2.13. Cryo-Transmission Electronic Microscopy (Cryo-TEM)

RW16 was mixed with DOPC or DOPG LUVs (1 mM) in Tris buffer for a final peptide concentration of 40 μM (P/L ratio of 1/25). After 1 h incubation, a 5 μL sample was deposited onto a lacey carbon cupper grid (Ted pella) placed in the automated device for plunge-freezing (EM GP Leica) enabling a perfect control of temperature (15 °C) and relative humidity (70%). The excess of sample was blotted with filter paper and the grid was plunged into a liquid ethane bath cooled and maintained at −183 °C with liquid nitrogen. Specimens were maintained at a temperature of approximately −170 °C, using a cryo holder (Gatan, CA, USA) and observed with a FEI Tecnai F20 electron microscope operating at 200 kV and at nominal magnifications of 19,000× or 50,000× under low-dose conditions. Images were recorded with a 2k×2k USC 1000 slow-scan CCD camera (Gatan) and analyzed using ImageJ.

3. Results and discussion

The choice in terms of the model membrane lipid composition used in each experiment has taken into account several aspects among which the typical composition of the cell membrane to mimic and the limitations of the technique employed. Eukaryotic cell membranes contain essentially zwitterionic lipids such as phosphatidylcholine lipids (PC) so this kind of lipid was used to mimic those cells. Several studies have shown that the cell membrane composition changes in cancer cells with overexpression of certain types of proteoglycans and the enrichment in the outer leaflet of negatively charged lipids (such as phosphatidylserine, PS) [15,16,18,19]. Therefore, overall cancer cells possess a more negatively charged membrane than normal cells. In view of the potential of RW16 in decreasing the motility (migration speed, random motility coefficient, wound healing) of the tumor cells and its intracellular actin-remodeling activity [10], the study of the interaction of this peptide with membranes mimicking cancer cells is of interest. To mimic the cancer cell membrane negatively charged lipids such as phosphatidylglycerol (PG) and PS were used in the present studies. Additionally bacterial membranes are rich in negatively charged lipids such as PG and as will be presented below RW16 as antimicrobial activity. Depending on the limitations of each technique, the fatty acid chain length and degree of unsaturation was chosen accordingly.

3.1. Antimicrobial activity

The antibacterial activity of RW16 was assayed against Gram-negative and Gram-positive bacteria (Table 1). RW16 inhibited the growth of both Gram-positive and Gram-negative bacteria with minimal inhibitory concentrations in the low micromolar range. It is interesting to note that for peptide concentrations around the MIC value in the case of *S. aureus*, the bacteria appeared non-homogeneously dispersed in the plate being agglomerated in certain regions. This was not observed for the other two bacterial strains investigated. For *E. coli* and *S. aureus*, the lytic activity of RW16 was tested by incubating bacteria overnight with a RW16 concentration corresponding to the MIC. No colony-forming units appeared in the case of *E. coli*, indicating that RW16 is bactericidal. In the case of *S. aureus*, the bacteria were able to re-grow after being incubated with RW16 at the MIC concentration, demonstrating the bacteriostatic activity of RW16 on this bacterial strain.

3.2. Peptide effect on turbidity and homogeneity of membrane models

Turbidity experiments (Fig. 1) followed absorbance changes at 436 nm of vesicle suspensions of DOPC, DOPE, DOPG and DOPS LUVs upon gradual addition of RW16. We have observed that addition of peptide to zwitterionic (DOPC or DOPE) LUVs caused no changes in turbidity, whereas they lead to a massive increase in the turbidity of DOPG or DOPS LUVs indicating that vesicle aggregation occurred. This result shows that electrostatic interactions between negative charges of anionic membranes and the positive charges of RW16 (10 positive charges at pH 7) are inducing liposome aggregation. These results are not surprising since it has already been shown that cationic CPPs interact preferentially with negatively charged membrane [21,39–42]. When kinetic experiments were performed after the initial aggregation, a slow decrease in turbidity was observed after 3 min incubation (data not shown). This goes along the lines of a dissociation of the liposome aggregates with time, after the initial aggregation, rather than their fusion.

We also monitored the size of liposomes, following addition of peptide, by DLS to further understand the observed changes in LUVs turbidity (Table 2). We performed DLS experiments on RW16 alone to investigate whether the peptide auto-associates or not. In this case we have observed that below a concentration of 5 nM the size of the scattering particles was too small to be detectable but above this concentration the size rapidly increases to form objects with a size between 90 and 170 nm (data not shown). This indicates that RW16 rapidly forms oligomers at very low concentrations (concentrations comprised between 1 nM and 5 nM) probably due to high hydrophobic interactions between the Trp. RW16 being an amphipathic peptide, its autoassociation is expected and indeed was shown here to occur below a concentration of 5 nM. The experimental setup being different for each method used, the peptide was in the monomer form in some studies (PWR, calcein leakage) while in others was in oligomeric form (ITC, DSC, NMR, CD, Trp fluorescence). This aspect is important when analyzing the results as the nature

Table 1
Antimicrobial and lytic activities of RW16.[a] Results are the mean of three independent experiments each performed in duplicate.

Peptide	*E. coli*	*S. aureus*	*K. pneumoniae*
RW16	10 μM[b]	5 μM[c]	>100 μM

[a] The antimicrobial activity is expressed as MIC (μM), the minimal peptide concentration required for total inhibition of cell growth in liquid medium.
[b] Lytic effect observed at this concentration.
[c] No lytic effect observed at this concentration.

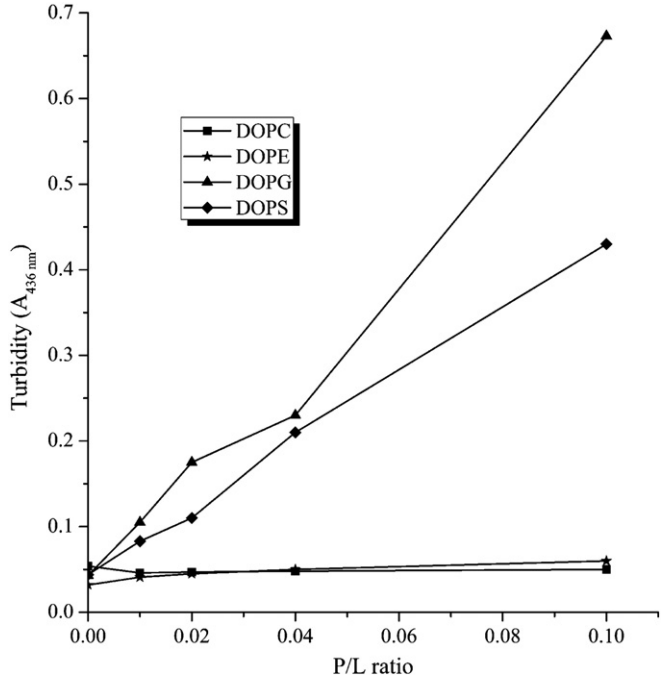

Fig. 1. Turbidity measurements of LUVs composed of DOPC, DOPE, DOPG and DOPS (all at 1 mg/mL in Tris buffer) following RW16 incremental addition (P/L ratios of 1/100, 1/50, 1/25 and 1/10 corresponding to 12.5 μM, 25 μM, 50 μM and 125 μM respectively). The experiments were performed in duplicate.

of the peptide exposed areas changes upon its oligomerization state. The monomeric form of the peptide has both hydrophobic and hydrophilic surfaces exposed. Peptide autoassociation should occur through the hydrophobic face, so the oligomer will have a hydrophobic core (mostly not accessible) and a hydrophilic available surface. In fact, fluorescence experiments were performed to compare the λ_{max} of RW16 with that of penetratin, a peptide that has not been shown to oligomerize. The λ_{max} of the Trp fluorescence of RW16 alone was slightly shifted (347 nm) compared to that of the penetratin alone (350 nm, data not shown).

DLS experiments on liposomes show that DOPC vesicle size did not change upon peptide addition. In the case of DOPE LUVs the polydispersity index was too high to be able to exploit the data but it seems that larger or different objects were formed. This could be due to the propensity of PE to form inverted micelles as it has been observed by Seddon [43]. In the case of DOPS and DOPG LUVs, a significant increase of the liposome size that could reach about 1 μm of hydrodynamic radius was observed. Measurements were taken immediately after peptide addition to liposomes and an increase in the solution turbidity was seen right away. After several days, a lipid deposit at the bottom of the tubes was formed. Thereby, one can assume that electrostatic interactions between the peptide and the lipid play an important role in liposome behavior in terms of homogeneity and aggregation. Similar behavior was observed in the case of RL16, a peptide with the same sequence but with Leu residues instead of Trp [21]. Other CPPs such as penetratin, and arginine-rich peptides as well as antimicrobial peptides which also possess a great amount of positively charged residues also show important electrostatic interactions with anionic lipids [21,39–42,44]. From the data we cannot yet predict whether the larger objects observed arise from liposome aggregation or fusion.

To better understand the peculiar behavior of PE liposomes in the presence of the peptide (no changes in turbidity but increase in particle sizes), we have performed ^{31}P NMR on DOPE MLVs in the absence or presence of RW16 (Figs. 2 and S2). The peptide was added to the liposomes at a P/L ratio of 1/100 and temperature was scanned from 2 to 20 °C. We have observed that the transition from the lamellar phase (Lα) to the hexagonal type II phase (H_{II}) occurred at 7.1 °C ± 0.4 °C and in the presence of RW16 at 11.1 °C ± 0.4 °C. This result shows that the peptide stabilizes the lamellar phase, which could be explained by an intercalation of the peptide between the lipid polar headgroups without insertion into the bilayer core. This location would counteract the natural effect of PE lipids to induce a local negative curvature prompting for hexagonal type II phases. It also appears that the peptide promotes a small percentage of isotropic phases (sharp peak centered at 0 ppm). This would suggest that the RW16 peptide promotes in addition a limited, but detectable, membrane restructuration with appearance of μm-sized MLVs. To conclude RW16 interacts, in a moderate way, with PE lipids.

Table 2
Vesicle size distribution from Dynamic Light Scattering measurements of LUVs composed of DOPC, DOPE, DOPS and DOPG expressed as the hydrodynamic diameter (nm). The lipid concentration was 1 mg/mL to which peptide was gradually added. The experiments have been done in duplicate at room temperature.

P/L ratio	DOPC	DOPE	DOPS	DOPG
0	120 ± 10	145 ± 15	115 ± 5	120 ± 10
1/100	122 ± 12	267 ± 107[a]	121 ± 11	133 ± 19
1/50	116 ± 6	472 ± 252[a]	140 ± 30	261 ± 100[a]
1/25	121 ± 11	757 ± 7	141 ± 31	302 ± 64[a]
1/10	125 ± 15	759 ± 440[a]	1235 ± 565[a]	1244 ± 284[a]

[a] The error bars were too important to establish an exact size of the liposomes.

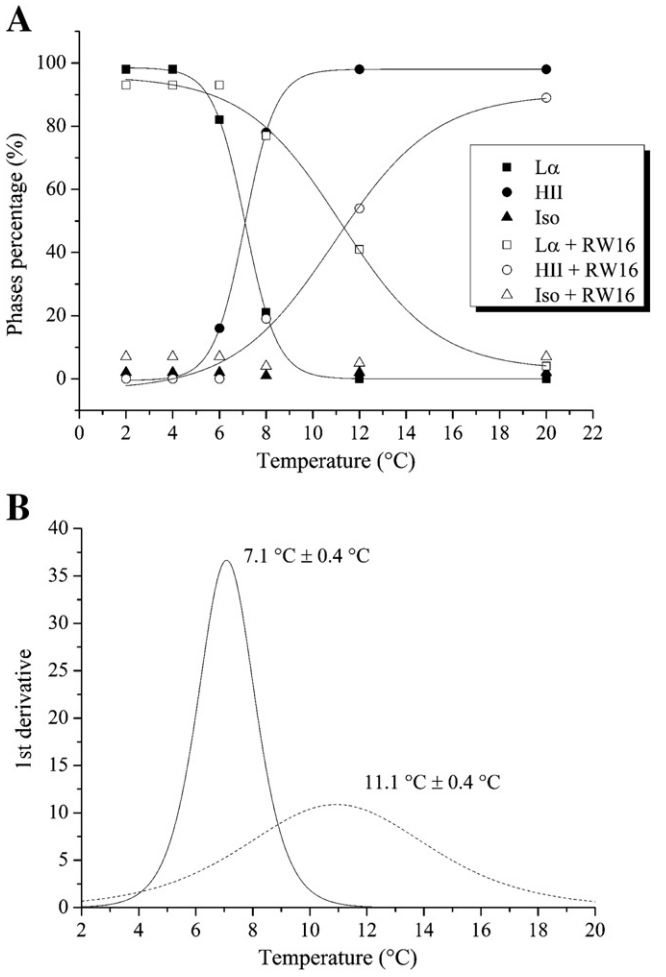

Fig. 2. (A) Percentages of lamellar (Lα), hexagonal type II (HII) and isotropic (Iso) phases of DOPE as a function of the temperature in the absence (filled symbols) and presence (empty symbols) of 1/100 of RW16 (2 mM). The points were fitted through a sigmoidal curve. (B) First derivative of the percentages of lipid phases represented in A in the absence (solid line) and presence (dashed line) of RW16 at P/L 1/100.

3.3. Peptide effect on lipid organization and membrane integrity

The interaction of RW16 with phospholipids was studied by monitoring the way this peptide affects the Lβ gel phase to the Pβ′ ripple phase (pre-transition temperature, T_{pre}) and the Pβ′ ripple phase to the Lα liquid phase (main transition temperature, T_m) transitions of different lipids. Indeed, the phase transition temperature and thermodynamics of lipid phase transitions are extremely sensitive to the presence of exogenously added compounds. Herein, we have chosen to use C14 fatty acyl chain lipids as their phase transition is close to room temperature, which facilitates handling (reason why they are often used in DSC studies, despite their absence in cell membranes). The experiments were performed with MLVs rather than other type of vesicles because MLVs give a higher magnitude and more homogeneous signal in DSC [45]. DSC heating endotherms illustrating the effect of RW16 on MLVs of DMPC, DMPC/Chol (95:5), DMPG, DMPG/Chol (95:5), DMPG/DPPC (60:40) are presented in Fig. 3 and the thermodynamic parameters obtained from these experiments are presented in Table 3.

Vesicles of DMPC exhibit two endothermic events, a less energetic pre-transition near 14 °C that arises from the conversion of the Lβ to the Pβ′ phase and a more energetic main transition from the conversion of Pβ′ to Lα phase around 24 °C. In interaction with DMPC (Fig. 3A, Table 3) the peptide decreases the pre-transition enthalpy (ΔH_{pre}) starting from very low concentrations (P/L = 1/100). This decrease in the pre-transition enthalpy arises from a modification in the tilting of the lipid polar headgroups and shows an interaction between the peptide and the lipid polar headgroups. As for the main transition, RW16 does not significantly change the T_m but reduces the main transition enthalpy (ΔH_m) and increases the $\Delta T_{1/2}$. A change in ΔH_m is the consequence of the disruption of van der Waals interactions between the hydrocarbon chains. It shows that the peptide is able to intercalate between the fatty acid chains reducing the cooperativity of the transition (reflected in the increase of the $\Delta T_{1/2}$).

In terms of the pre-transition, RW16 affects strongly that of DMPG than DMPC, as it completely abolishes it, starting at very low concentrations (P/L = 1/100) (Fig. 3B, Table 3). This may be a consequence of the more favorable electrostatic interaction between the negatively charged lipid headgroup and the positive charges in the peptide. At increasing concentrations of peptide we have observed a splitting of the main transition peak which has been suggested in the literature to arise from the coexistence of peptide-rich and peptide-poor domains in the bilayer [46,47]. We have observed an increase of the $\Delta T_{1/2}$ which arises from a decrease of the cooperativity of the hydrocarbon chains due to the insertion of the peptide in the lipids.

While the role of electrostatics could be studied by just comparing the effect of the peptide on zwitterionic vs anionic lipid membranes (using single lipid liposomes), binary lipid mixtures containing lipids with sufficiently different phase transition temperatures have been used to evaluate the possible lipid recruitment induced by the peptide [48–50]. Herein we have worked with vesicles composed of DMPG/DPPC (60:40). We have to remind that the T_m of DMPG and DPPC are 24 °C and 41 °C, respectively. As presented in Fig. 3C the binary mixture presents a T_{pre} around 19.1 °C and a T_m around 30.9 °C. In interaction with these vesicles the peptide induces a splitting of the

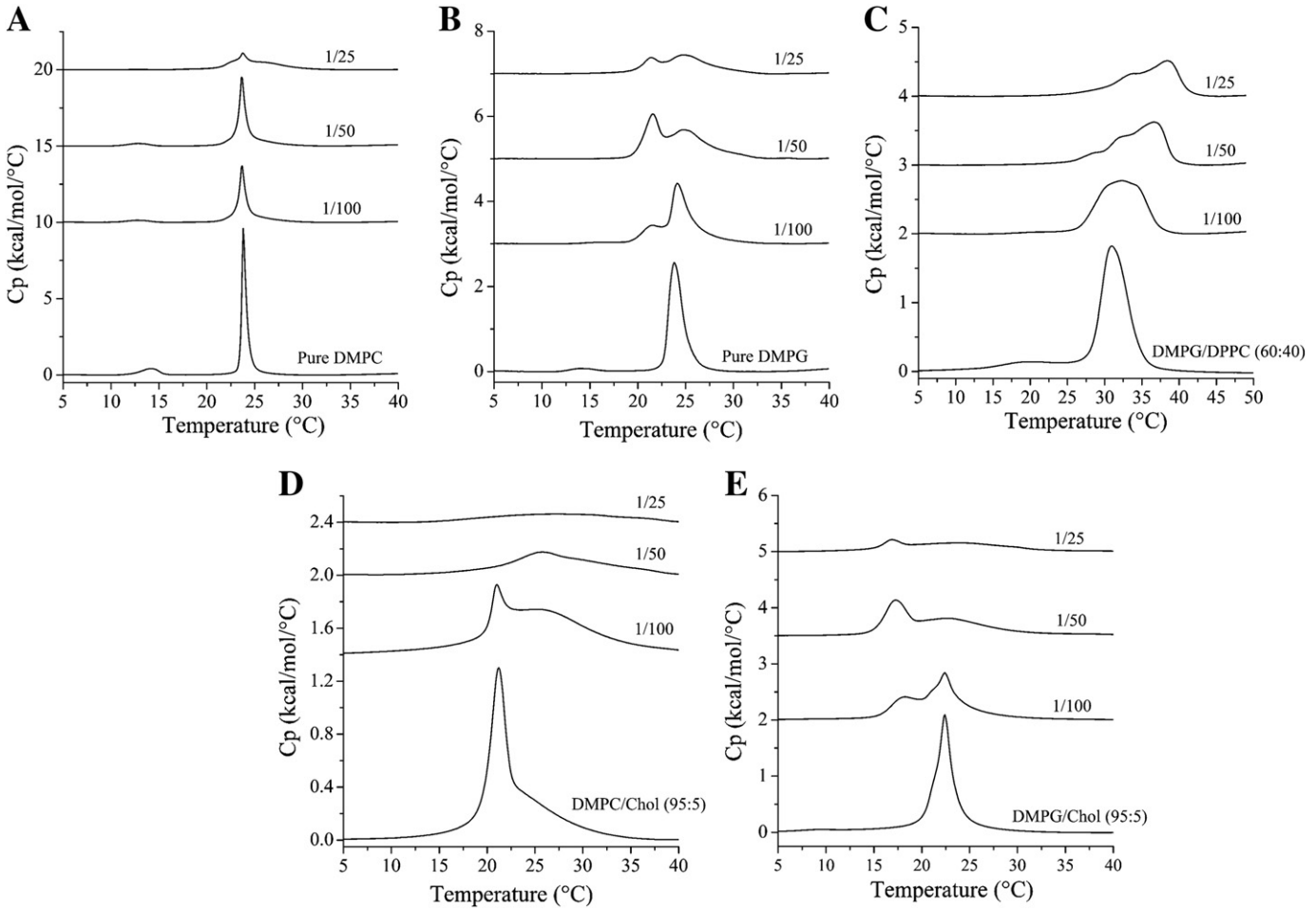

Fig. 3. DSC thermograms illustrating the effect of the addition of increasing concentrations of peptide to DMPC (A), DMPG (B), DMPG/DPPC (60:40) (C), DMPC/Chol (95:5) (D) and DMPG/Chol (95:5) (E) vesicles.

Table 3
Thermodynamic parameters obtained with DSC experiments. For all experiments at least 4 scans were done in order to attain thermodynamic equilibrium. Two values indicate a splitting of the signal.

		Pre-transition				Main transition			
		T_{pre} (°C)	ΔH (kcal/mol)	ΔS (cal/K/mol)	$\Delta T_{1/2}$ (°C)	T_m (°C)	ΔH (kcal/mol)	ΔS (cal/K/mol)	$\Delta T_{1/2}$ (°C)
DMPC	Lipid	14.2	1.4	3	2	23.8	8.7	29	0.5
	1/100 RW16	12.7	0.6	2	2.6	23.7	6.2	21	0.8
	1/50 RW16	12.8	0.5	2	2.5	23.7	5.4	24	0.8
	1/25 RW16	12.9	0.1	0	3	23.7/26.5	2.9/2.5	9.8/8.3	2.2/4.2
DMPG	Lipid	14.3	0.3	1	3	23.8	6	20	1.5
	1/100 RW16	–	–	–	–	21.5/24.1	0.6/4.8	2/16	1.4/2.3
	1/50 RW16	–	–	–	–	21.6/24.8	2.2/4.4	7.5/15	1.5/4.2
	1/25 RW16	–	–	–	–	21.4/25	1.3/3.7	4.4/12	1.5/5.2
DMPG/DPPC (60:40)	Lipid	19.1	0.4	1	5.5	30.9	9	30	3.8
	1/100 RW16	–	–	–	–	32.2	6.5	21	6.9
	1/50 RW16	–	–	–	–	32.9/36.4	4.4/2.3	14/11	6.7/2.8
	1/25 RW16	–	–	–	–	34/38.4	2.82/2.13	9.2/6.8	5.94/2.97
DMPC/Chol (95:5)	Lipid	–	–	–	–	21.2/24.9	3.4/2.7	12/9.1	1.8/7.1
	1/100 RW16	–	–	–	–	21.1/25.8	0.7/6.2	2.4/21	1.4/10.9
	1/50 RW16	–	–	–	–	25.6/31.6	1.8/0.6	6/2	7.3/7.1
	1/25 RW16	–	–	–	–	27.3	3.5	12	22.9
DMPG/Chol (95:5)	Lipid	13.6	nd	nd	nd	22.4	5.8	20	1.9
	1/100 RW16	–	–	–	–	22.4/18	3.9/1.3	13/4.4	3.4/2.6
	1/50 RW16	–	–	–	–	23.2/17.3	4.1/2	14/6.9	8.6/2.2
	1/25 RW16	–	–	–	–	23.8/16.9	3.4/0.5	11/1.7	12.5/1.9

– The transition was not observed.

main transition peak at a P/L ratio 1/50. One peak is displaced to higher temperatures when increasing concentrations of peptides are added approaching the main transition of the DPPC (41 °C). This means that the peptide leads to the segregation of DPPC from the lipid mixture. Consequently the other peak, observed at a lower temperature, corresponds to the peptide-perturbed phase transition of DMPG. Since the T_m of the DMPG-rich component is further away from the T_m of DMPG pure (about 10 °C difference for P/L 1/25) than that of the DPPC-rich component from DPPC pure (less than 2 °C of difference for P/L 1/25), the DMPG-rich component is more affected, so more enriched in peptide. One should note that each lipid-rich component is not expected to possess a T_m exactly similar to the T_m of its main lipid component (even if no peptide is affecting its transition), this is because each component is not purely composed of its main lipid as there is always some of the other lipid component mixed. The data points to a preferential interaction of RW16 with a domain rich in DMPG and a segregation of a DPPC rich component. The driving force behind this peptide preference for DMPG might be either electrostatic and/or the greater fluidity of this lipid as we have observed in previous studies, where the preferential peptide interaction occurred with the lipids possessing lower T_m [51]. Studies by other laboratories using DSC have also shown a preferential interaction of a peptide with one lipid component in a binary mixture and the consequent segregation of the other component [48–50].

When cholesterol is present in the DMPC vesicles (5%) the pre-transition is not observable (Fig. 3D, Table 3). Indeed cholesterol, by fluidifying the membrane, highly decreases the enthalpy of the phase transition abolishing the pre-transition signal and highly broadening the main transition. The main transition peak (around 21.2 °C) is splitted when the peptide is added, the enthalpy highly decreases and the $\Delta T_{1/2}$ highly increases. In the presence of cholesterol (DMPC/Chol 95/5% mol/mol) the decrease in enthalpy is considerably more important than in the case of DMPC vesicles (we have observed a decrease in enthalpy of 80% with DMPC/Chol and 46% with DMPC alone). The higher decrease in the cooperativity of the main transition observed in the presence of cholesterol shows that the peptide affects more the fatty acid chain packing in the presence of cholesterol. This suggests that cholesterol, by inducing the formation of a liquid ordered phase (Lo) in the membrane, improves peptide insertion into the bilayer. In the case of DMPG/Chol (95/5% mol/mol) vesicles, the behavior of the lipids with increasing concentrations of peptide is practically the same as that observed for DMPG alone (both in terms of enthalpy and cooperativity of the transition) (Fig. 3E). The fact that the presence of cholesterol does not change the mode of interaction of RW16 with anionic lipids suggests that the peptide penetrates less deep in the fatty acid chain region in the presence of anionic lipids vs zwitterionic ones.

The membrane perturbation effect of the peptide was then investigated by calcein leakage experiments. LUVs composed of DOPC, DOPG and DOPC/DOPG (8:2) were used and P/L ratios in the range of 1/1000 to 1/10. Smaller P/L ratios were used here (P/L 1/1000) compared to other experiments (usually the smallest P/L ratio was 1/100) because calcein leakage started to occur at very low concentrations. Contrarily to previous experiments, here lipids with C18:1 fatty acid chains were used to ensure that lipids were in the fluid phase at room temperature (the T_m of these lipids is inferior to 0 °C). For this kind of experiments if lipids are in the gel phase the calcein leaks automatically due to the rigidity and defects of the bilayer. In the absence of RW16 a low fluorescence signal was observed due to calcein self-quenching inside the liposomes, no leakage from liposomes occurred under these conditions (Fig. 4A). Kinetic experiments show that RW16 leads to a very fast leakage that occurs in a matter of seconds and that saturates in about 2 h (P/L ratio 1/25, Fig. 4A, Ft). When the peptide was incrementally added to DOPC LUVs a strong increase in the percentage of calcein leakage was observed starting from very low P/L ratio (1/1000). Additionally, the signal saturated at very low peptide concentration (~20 nM, P/L ratio 1/50) (Fig. 4B). When monitoring the changes in calcein leakage using different peptide concentrations, one can see that leakage started to occur at very low concentrations of RW16 (1 nM) and that it rapidly reached saturation (with a leakage of ~75%) for a concentration of peptide of 40 nM (which corresponds to P/L = 1/25). The plot was fitted through a hyperbolic curve allowing determination of a half maximum activity of 3.2 ± 0.7 nM. The leakage process seems to be cooperative, as it has already been observed by other laboratories. Indeed it has been shown that cooperative insertion of the peptide could occur. This peptide insertion (only few peptide molecules are sufficient) would create a mass imbalance and membrane destabilization [52]. This mass imbalance has also been demonstrated using molecular dynamics simulations as a mechanism responsible for strong membrane perturbation leading to formation of membrane defects [53–55].

The calcein leakage behavior of DOPG liposomes is more complicated to analyze. While at low concentrations (up to 40 nM that corresponds to a P/L of 1/25) there is less leakage than with DOPC and

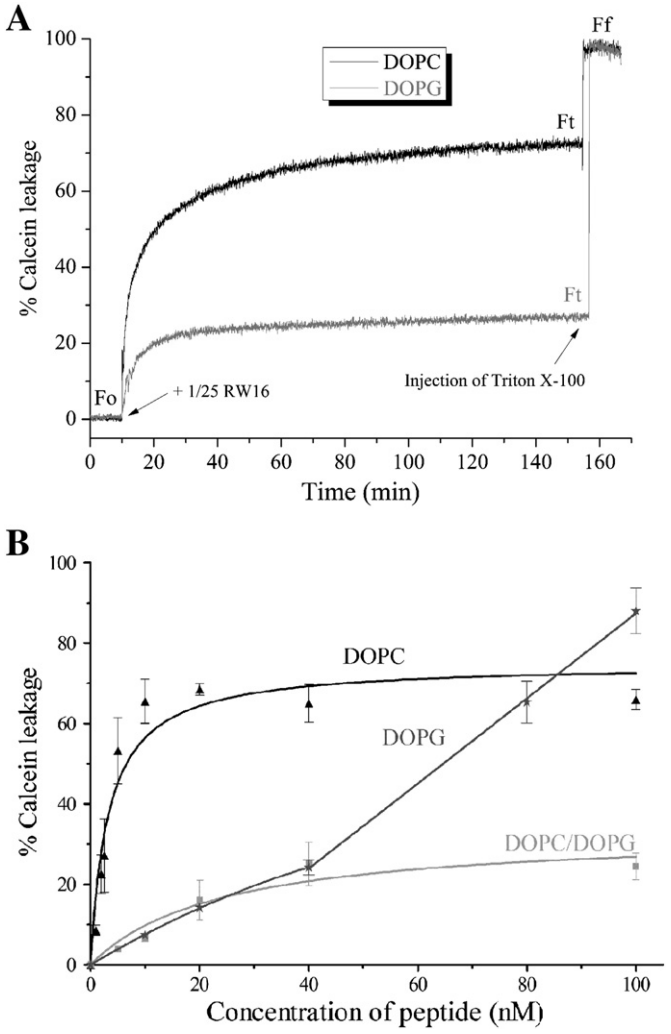

Fig. 4. (A) Typical fluorescence measurements for a calcein leakage experiment. The peptide is added (in this case with a P/L ratio of 1/25) to LUVs after ~10 min to check any basal leakage (Fo) and Triton X100 is added at the end of the measurement (Ff), that is after ~2.5 h to obtain the maximum liposome leakage (Ft). (B) Calcein leakage from DOPC (black), DOPG (dark gray) and DOPC/DOPG (80:20) LUVs (gray) upon peptide addition in the range 0–100 nM. All data were fitted using a hyperbolic curve, except in the case of DOPG where a two phases fit (hyperbolic and linear) was performed. Error bars mean SEM on at least 3 experiments.

the response is hyperbolic although much less cooperative, at high concentrations (above P/L 1/25) the response is linear and strong leakage is observed. This data has to be taken with caution as it has been observed by DLS and turbidity that strong perturbations in anionic liposomes size occur at high P/L ratios with aggregation of objects. When the vesicles were composed of DOPC/DOPG (8:2) the profile of the curve is very similar to that of DOPG at low peptide concentrations indicating that the peptide is first interacting with anionic lipids in a cooperativity manner. Once all the anionic lipids are occupied, the peptide interacts with zwitterionic lipids always in a cooperativity manner as observed in the case of DOPC alone. The percentage of leakage is similar to that of DOPG at low concentrations. This interpretation agrees well with that proposed in the DSC experiments on DMPG/DPPC LUVs (Fig. 3C, Table 3) and reinforces the anionic lipid segregation theory. Furthermore it could suggest that the higher the complexity of lipid model composition, the less they are susceptible to perturbation compared to model membranes composed of single lipids. Although these effects may partly be due to specific interactions between the peptides and the phospholipid headgroups, they also suggest a competition between electrostatic and hydrophobic forces. For a bilayer consisting of zwitterionic phospholipids, these peptides could possibly be inserted more deeply into the hydrophobic part of the bilayer (through the hydrophobic peptide face containing the Trp residues) causing an important leakage. In the case of negatively charged lipids, the electrostatic attraction between the peptide and the lipid (in this case the charged peptide face would be facing the lipid headgroups) could "immobilize" the peptide in the lipid headgroup region inhibiting a deeper insertion. Similar observations have previously been reported for the bee venom melittin [56].

3.4. Peptide affinity for the membrane

The affinity of RW16 for bilayers purely zwitterionic or composed of both anionic and zwitterionic lipids (eggPC/POPG and DOPC/DOPS) was studied by PWR (Fig. 5) and the resulting dissociation constants are presented in Table 4. Successive aliquots of RW16 solutions were added to the sample compartment of a PWR cell containing preformed bilayers composed of each of the different lipids used in these experiments. The signals observed before and after bilayer formation and upon saturating concentrations of peptide for *p*- and *s*-polarization are presented in Fig. 5 panels A and B, respectively. From these spectra we can get different information relative to the system deposited on the prism surface by analyzing the shift of the minimum of reflectance as a function of concentration or by fitting the spectra to obtain the optical parameters (for more details, see [57]). In all cases, PWR spectral changes were observed upon peptide addition to the membrane, indicating peptide interaction with the bilayers. In our case when the peptide is added to the bilayer we have observed a decrease in the mass of the system (as the angle of resonance decreases for both polarizations, $\Delta\alpha<0$) and a decrease of the thickness of the system (as the spectral depth decreases, $\Delta R<0$). A simple molecular interaction should lead to an increase in the resonance angle position as an increase in mass is produced by the interaction of additional molecules with the prism surface (increase in the refractive index). When this is not the case, it means that the peptide leads to a reorganization of the bilayer resulting in removal of part of the lipid mass from the membrane. Two explanations are possible for this scenario: the peptide has a detergent effect on the membrane, solubilizing part of the bilayer or the peptide leads to changes in the lipid properties resulting in a higher surface area occupied by each lipid molecule (and so a reduced mass per surface). At this stage it is not possible to distinguish between the two explanations.

A typical plot of the resonance angle changes for *p*- and *s*-polarization as a function of added concentrations of RW16 for an eggPC bilayer is shown in Fig. 5C. These points can be fitted through a hyperbolic function indicating that saturable binding occurred. Apparent dissociation constants are presented in Table 4. As mentioned above this experiment was conducted in bilayers purely zwitterionic and containing also anionic lipids. In all cases, RW16 induced shifts to smaller angles, indicating that in all cases a reorganization of the membrane occurred with a decrease in the mass of the system. Using Eqs. (2) and (3), the contributions of a pure mass effect and a pure structural effect to the spectra were calculated, indicating that mass changes accounted for 80–100% of the spectral changes (~100% in the case of eggPC and DOPC bilayers and ~90% and ~80% in the case of a mixture of DOPC/DOPS or eggPC/POPG bilayers, respectively). As for our surprise, the affinity constants obtained show that the affinity of RW16 for the lipids is mostly not affected by the lipid composition, being always in the low nM range. It is interesting to note that these values correlate very well with those obtained in calcein leakage experiments. Therefore, the dissociation constants observed by PWR reflect mostly the membrane perturbation exerted by the peptide on the membrane (pore formation or partial membrane disruption) rather than a simple membrane recognition (such as an electrostatic interaction between the positively charged amino acids in the peptide and the negatively lipid headgroups) which explains the lack of lipid specificity in the interactions. A decrease in

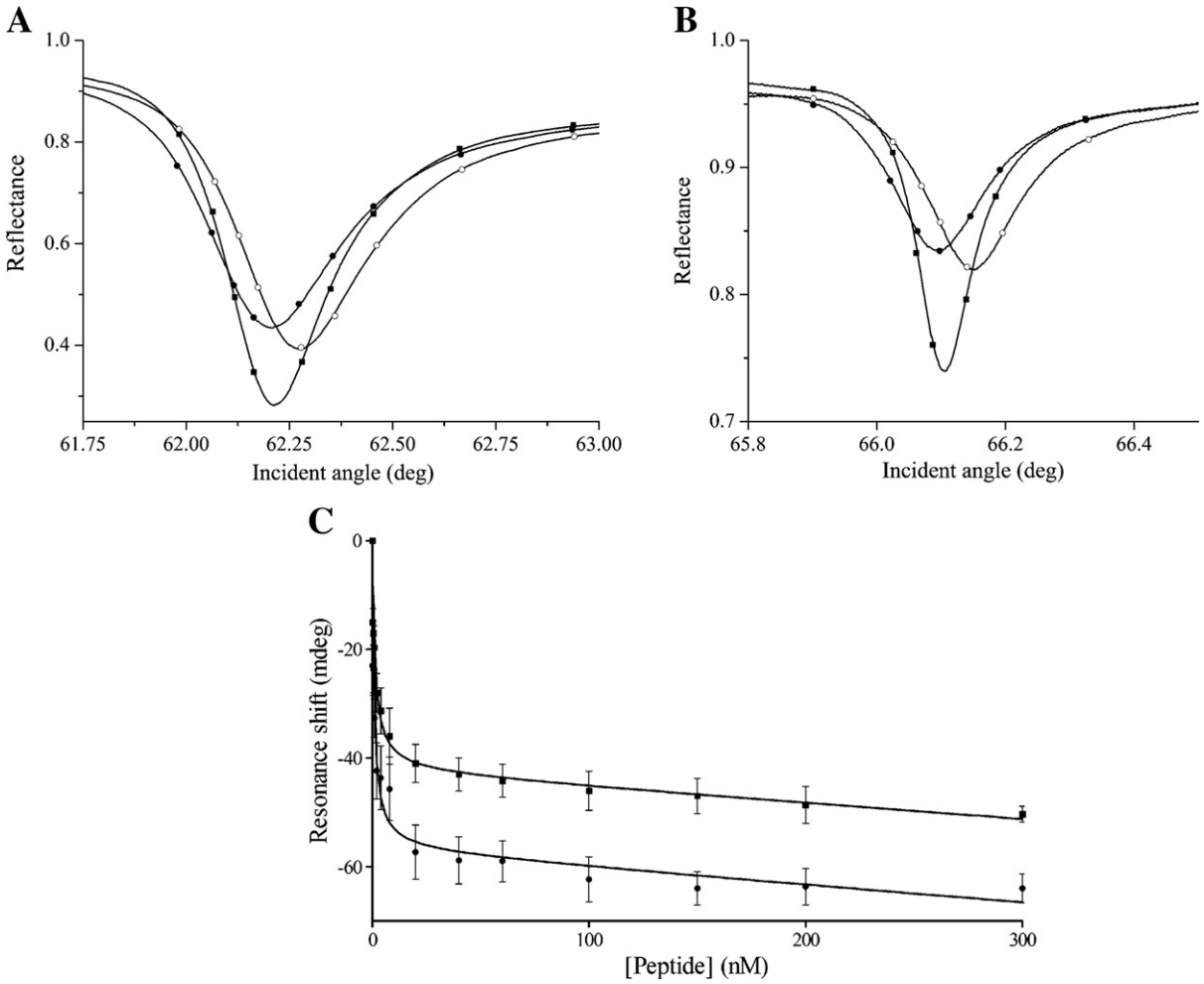

Fig. 5. Interaction of RW16 with an eggPC bilayer monitored by PWR. Panels A and B correspond to the PWR spectra obtained for the buffer (■), for the lipid bilayer (○) and after addition of 0.3 μM of RW16 to the bilayer (●) obtained for *p*- and *s*-polarized light, respectively. Experiments were performed with a spectral angular resolution of 1 mdeg. The shifts in the minimum of resonance upon incremental addition of peptide are presented in panel C for an eggPC bilayer. The points were fitted through a hyperbolic curve.

the bilayer thickness has been observed for other peptides and seems to be a common way of membrane destabilization by several membrane active peptides [58,59].

The affinity of RW16 to DOPG and DOPC LUVs was studied using Isothermal Titration Calorimetry. In these experiments RW16 solution (0.1 mM) was titrated with LUV solution (12.6 mM) and gradual injections were realized with 10 min interval between each injection to allow equilibrium. When DOPC vesicles were used no signal was observed (no heat exchange was developed for each injection; data not shown) contrarily to DOPG LUVs where a well defined exothermic signal was observed (Fig. 6A and B). An affinity in the micromolar range was determined from this data (Fig. 6, Table 5). The experiments have been done at different temperatures in order to determine the variation in the heat capacity (ΔCp, obtained from the slope of the linear fit) that reveals important information regarding the nature of the peptide/lipid interactions. The temperature dependence of ΔH is represented in Fig. 6C. The ΔCp is the sum of two terms resulting from the release of water from the hydrophilic and hydrophobic regions of the bilayer. When the $\Delta Cp > 0$ typical of electrostatic interactions, the enthalpy is "favorable", and when the $\Delta Cp < 0$ the interaction is "entropy driven" and this is typical of hydrophobic interactions which means a transfer of a molecule from a polar to a nonpolar environment. The ΔCp observed is negative (−42 kcal/mol/K) indicating that dehydration of hydrophobic regions of the bilayer is occurring during peptide interaction, hydrophobic interactions occupying an important role [60]. This correlates well with PWR results that have shown that the affinity of the peptide for lipids is not driven by the lipid charges. We have observed that the stoichiometry (n) increases with the temperature. We hypothesized this to be due to a decrease in the oligomerization state of the peptide at increasing temperatures (peptide dissociation).

One important aspect to note concerns the difference in the binding affinity range observed in the different experiments (in the nanomolar range with PWR and calcein leakage experiments and in the micromolar range with ITC experiments). We are most certain that the disparity in these results arises from the different experimental conditions used, more specifically concerning peptide concentration and thus peptide oligomerization state. As the DLS studies show, RW16 behavior (in the absence of lipid) changes depending on its concentration, with peptide autoassociation occurring around 5 nM. In PWR and calcein leakage

Table 4
Dissociation constants of RW16 for different lipid bilayers as determined by PWR. The experiments have been done at least three times.

	p-Polarization (nM)	*s*-Polarization (nM)
EggPC	1 ± 0.3	1.4 ± 0.4
EggPC/POPG	1.08 ± 0.3	0.6 ± 0.3
DOPC	1.68 ± 0.4	2.15 ± 0.6
DOPC/DOPS	2.2 ± 0.6	1.2 ± 0.5

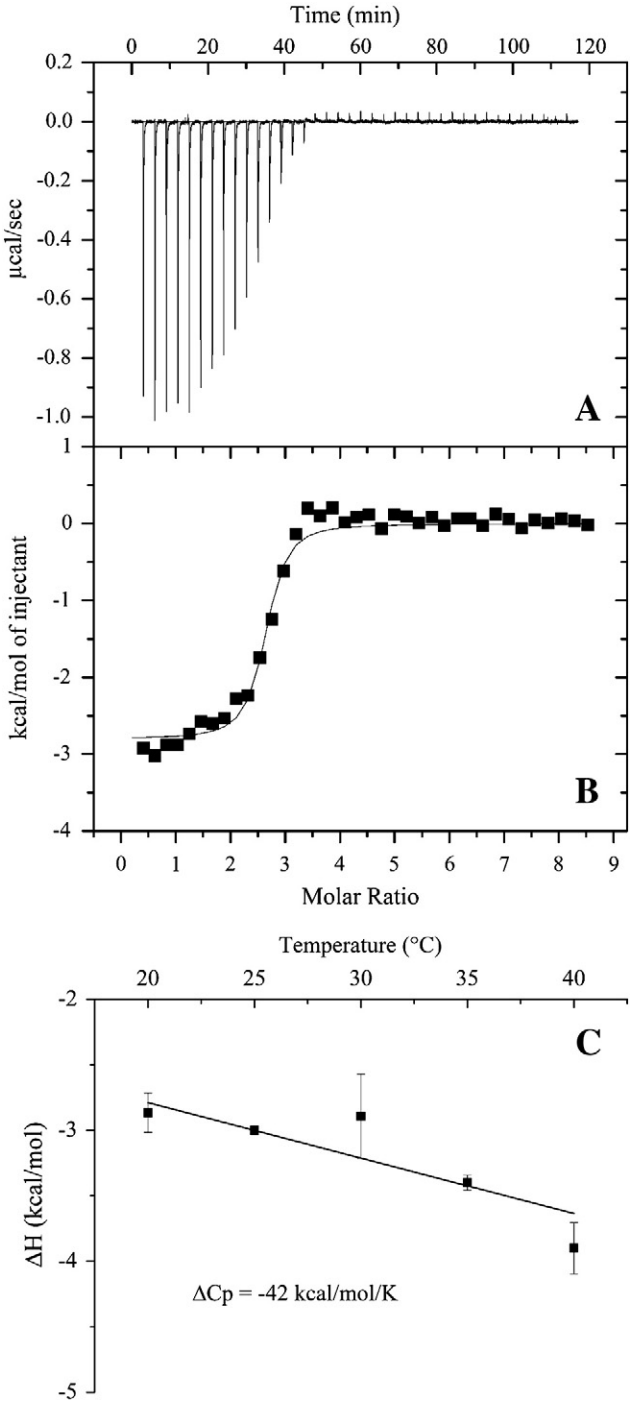

Fig. 6. Titration of the peptide solution (0.1 mM) with 2.5 µL aliquots of DOPG LUVs (12.6 mM) (A) and the corresponding integrated signals (B) for a temperature of 20 °C. The temperature dependence of the binding enthalpy for the interaction between DOPG LUVs and RW16 is presented panel C. The ΔCp corresponds to the slope of the linear fit.

Table 5
Thermodynamic parameters obtained from the ITC experiments. The solution of peptide (0.1 mM) was titrated with the solution of DOPG liposomes (12.7 mM). The experiments have been performed at different temperatures and averaged over two experiments.

T (°C)	n	*Kd* (µM)	ΔH (cal/mol)	ΔS (cal/mol/°C)	ΔG (cal/mol)
20	2.32	1.7	−2866	16.6	−3198
25	3.4	1.3	−3004	16.8	−3424
30	3.7	6.7	−2892	14.1	−3315
35	6.8	2.7	−3403	14.4	−3907
40	6.7	18	−3976	9.02	−4337

experiments the peptide is added to the liposomes starting from low peptide concentrations (the peptide being in the monomer form) whereas in the ITC experiments the liposomes are added to the peptide that is at 0.1 mM so already auto-associated. While at low peptide concentrations, the peptide has both faces (hydrophilic and hydrophobic) exposed for lipid interaction and can therefore interact with both zwitterionic and anionic lipids with increased affinity (as observed in PWR studies), at higher peptide concentrations the peptide hydrophobic face is mostly buried (peptide autoassociation) and so the P/L interactions are mostly hydrophobic and so weaker (ITC results). This explains why no signal was observed in ITC using DOPC vesicles, while an interaction was observed by PWR. This will be further discussed in the conclusion section where a model is proposed to explain RW16 mode of action.

The fluorescence of Trp has been studied to follow the change in the Trp environment of RW16 following peptide/lipid interaction (Fig S1). RW16 fluorescence was monitored alone and upon contact with LUVs composed of either DOPC or DOPG or both DOPC/DOPG (8:2). The peptide concentration used was 0.5 µM, concentration at which the peptide is oligomerized. In all cases a shift of the λ_{max} was observed toward lower wavelengths (called "blue-shift" or hypsochromic shift) and an increase of the fluorescence intensity occurred. A blue-shift reflects a change of environment of the Trp from a hydrophilic environment (buffer) to a hydrophobic environment due to membrane adsorption or insertion [61]. In a polar environment the λ_{max} is generally around 350 nm whereas in a nonpolar environment the λ_{max} is generally around 330–340 nm [61]. We have observed that in the presence of DOPG LUVs the final blue-shift is the same (from 347 nm to 338 nm; around 9 nm shift) but the concentration needed to reach the half-shift of the Trp emission spectrum is around ten times smaller in the case of DOPG LUVs than DOPC LUVs. This shift is consistent with the partitioning of the Trp side chain into a more hydrophobic, sterically confined environment. The change in the Trp environment to a more hydrophobic one can arise from peptide autoassociation where part of the Trp residues would be in contact with each other or from a burial of the Trp residue peptide in the lipid fatty acid chain region. At the concentration used here (0.5 µM), the peptide should be in the oligomer form. We hypothesize that in the presence of DOPG LUVs the peptide interacts with the membrane through electrostatic interactions, the accumulation of peptide at the membrane surface will lead to strong peptide/peptide oligomer repulsion and to a strong membrane destabilization. To release some of this electrostatic repulsion between the peptide oligomers, some of the peptide molecules will flip, inserting the Trp residues deeper in the membrane which explains the blue-shift observed. In the case of DOPC, the same mechanism will take place, that is the flip of the peptide molecules with the insertion of Trp in the lipid fatty acid chain region (same magnitude of blue-shift observed), the only difference being that here the concentration at which this would take place is higher as there is no electrostatic attraction with the lipid. Up to a certain concentration, the peptide would stay in solution, always in the form of oligomer, at increasing concentrations the charge–charge repulsions between the peptide oligomers in solution increase and so the peptide interacts with the membrane and flips to insert the Trp residues in the membrane. This flip around the Arg residues has been reported to occur in parent peptides, RL9 and RW9 (also amphipathic and with the same amino acid distribution but shorter than RW16) by molecular dynamic simulation studies [62]. In the mixture of DOPC/DOPG the concentration needed to reach the same 9 nm blue-shift is around the same observed for DOPG vesicles. So overall, the explanation is the same as that proposed for DOPG but in the presence of a mixture of PC/PG it appears that there is a competition between zwitterionic and anionic lipids. These results correlate well with calcein leakage and DSC experiments where an enhanced lipid perturbation by the peptide in the presence of anionic lipids occurs. Furthermore these results correlate well with ITC experiments showing the importance of hydrophobic interaction between peptide and lipid, compared to electrostatic interactions.

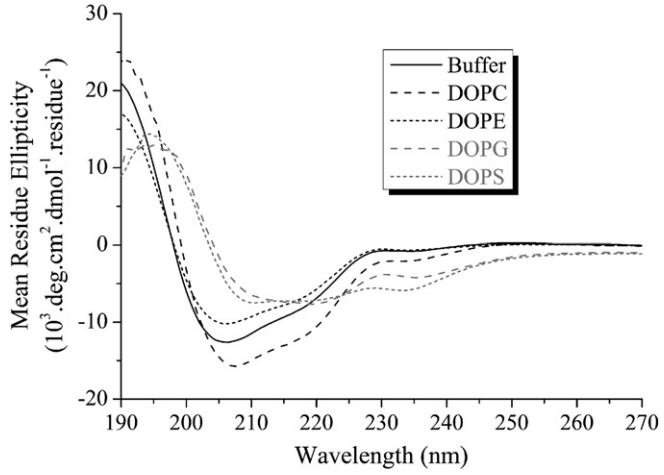

Fig. 7. CD spectra of RW16 in phosphate buffer and in the presence of LUVs of DOPC, DOPE, DOPG, and DOPS (1 mg/mL) at a P/L ratio of 1/25 (47 μM of RW16).

3.5. Structure of the peptide in contact with membranes

To determine whether the interaction of RW16 with membranes leads to structural changes of the peptide, circular dichroism experiments were performed in buffer (10 mM phosphate buffer) and in the presence of lipid vesicles of different compositions (zwitterionic DOPC or DOPE or anionic DOPG or DOPS LUVs) and at P/L ratios of 1/50, 1/25 and 1/10 (RW16 concentrations used varied from 24 μM to 111 μM). The peptide is thus in oligomeric form under all the conditions. The CD spectra are presented in Fig. 7. Analysis of CD spectra of RW16 in phosphate buffer demonstrated that the peptide is mostly structured in random coil (54%) and α-helix (46%). In the presence of zwitterionic lipids (DOPC or DOPE) the peptide secondary structure does not change significantly. Indeed the percentage of random coil is about 40% and the percentage of helix is about 60% with DOPC whereas the percentage of random coil is about 60% and the percentage of helix is about 40% with DOPE. In the presence of anionic lipids (DOPG and DOPS) the peptide seems to change its structure into a β-sheet. Indeed in the presence of DOPG or DOPS liposomes the percentage of random coil is about 40%, the percentage of helix is about 20% and the percentage of β-sheet is about 40%. As evidenced by Trp fluorescence blue-shift, these results show that RW16 binding to anionic lipids leads to a different secondary structure. Such structural change in the presence of anionic lipids may be induced by the strong accumulation in the membrane of peptide oligomers possessing highly charged surfaces and thus leading to the formation of aggregates with alterations in the peptide secondary structure. The conformational changes under membrane binding observed in our case are similar to those found in the literature for penetratin and

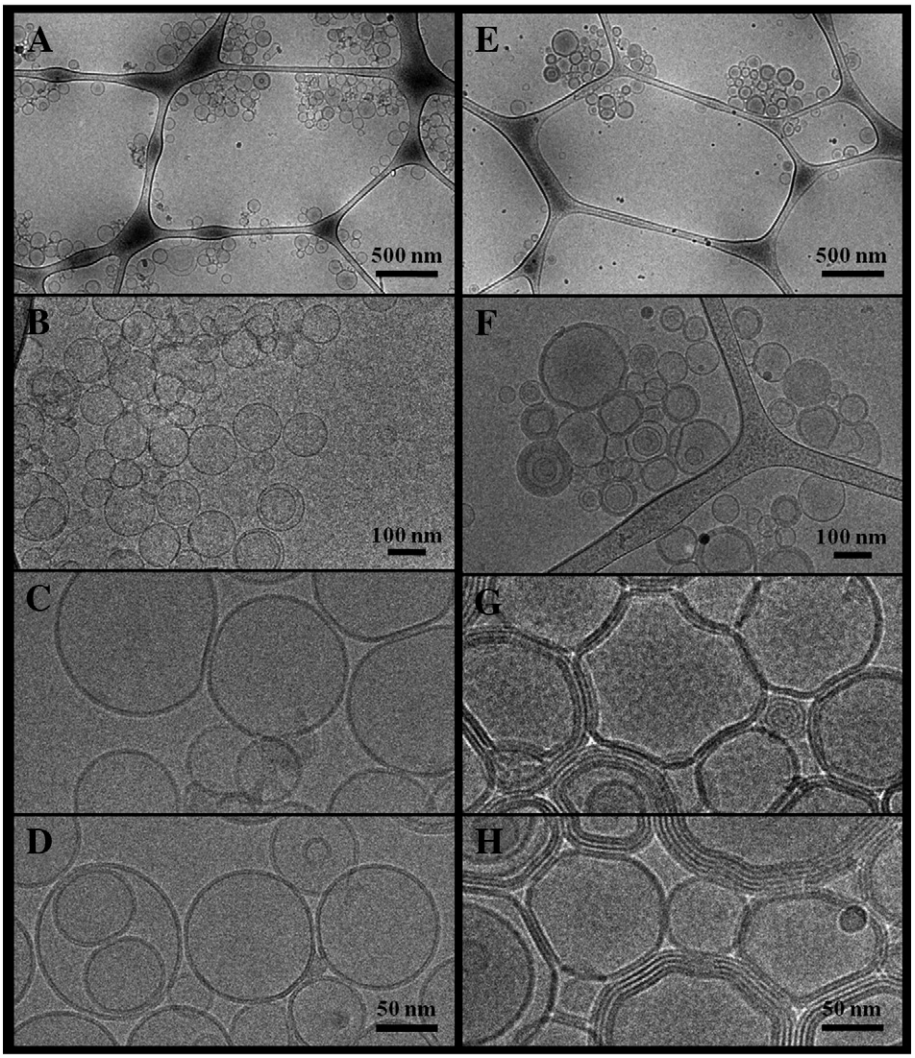

Fig. 8. Cryo-TEM pictures of DOPC (A to D) and DOPG (E to H) LUVs (both at 1 mM) with RW16 at a P/L ratio of 1/25. Scale bars are: 500 nm for A and E, 100 nm for B and F, and 50 nm for C, D, G and H.

other CPPs [63]. In this study they have explained the dependence of β-structure on the vesicle surface charge density by peptide aggregation. The higher negative charge density may be more effective in neutralizing the electrostatic repulsion between the positively charged peptides, hence facilitating interactions between them.

One can note that a broad band appears at 230–233 nm in all the spectra and that anionic membrane binding increases the intensity of this band. In the literature, studies on Trp-rich antimicrobial peptides (e.g., indolicidin) have attributed this signal to the Trp side chains which can be either positive or negative depending on the orientation of the Trp residues and their solvent exposition [64–66].

3.6. Cryo-TEM morphology analysis of liposomes in contact with the peptide

Cryo-TEM was used to provide morphological and supramolecular structural-information on membrane-bound RW16 assemblies, principally in the context of its membrane-perturbation and aggregation properties. Fig. 8 shows the representative images of DOPC LUVs (Fig. 8A to D) and DOPG LUVs (Fig. 8E to H) both with RW16 at P/L of 1/25. Fig. 8C and D shows that the morphology of zwitterionic liposomes is not affected by peptide addition. In the case of anionic lipids the result is quite different, the peptide largely deforms liposome structures and promotes liposome adhesion with great perturbation in the liposome curvature (Fig. 8G and H). The peptide enhances the contacts between the liposomes allowing them to deform and to create a more compacted arrangement. Thereby, the peptide acts as "glue" between anionic liposomes decreasing the membrane curvature tension. Another aspect that differs between the two liposomes concerns the general liposome distribution in the grid, while in the case of PC they appear more spreadly distributed (Fig. 8A) in the case of PG they are concentrated in more restricted areas and appear to form aggregates (Fig. 8E). Indeed one can observe that anionic vesicles are largely aggregated and this aggregation induced by RW16 leads to their deformation. Again, this enhanced membrane deformation observed in the case of anionic lipids agrees with the other studies presented. If one compares this data with previous data on penetratin [67,68], the peptide from which RW16 was derived, one can conclude that although both peptides highly perturb the lipid organization and membrane curvature, penetratin has a disordering effect on the membrane while RW16 seems to bring order in the membrane organization.

4. Conclusions

Herein, we have studied the interaction of a CPP with anti-tumor activity, RW16, with different lipid model systems. As mentioned above, RW16 has the capacity to autoassociate which changes and complicates data analysis. Equilibrium between the monomeric and oligomeric forms exists, low peptide concentrations (below 5 nM) favor the monomeric form and high concentrations (above 5 nM) favor

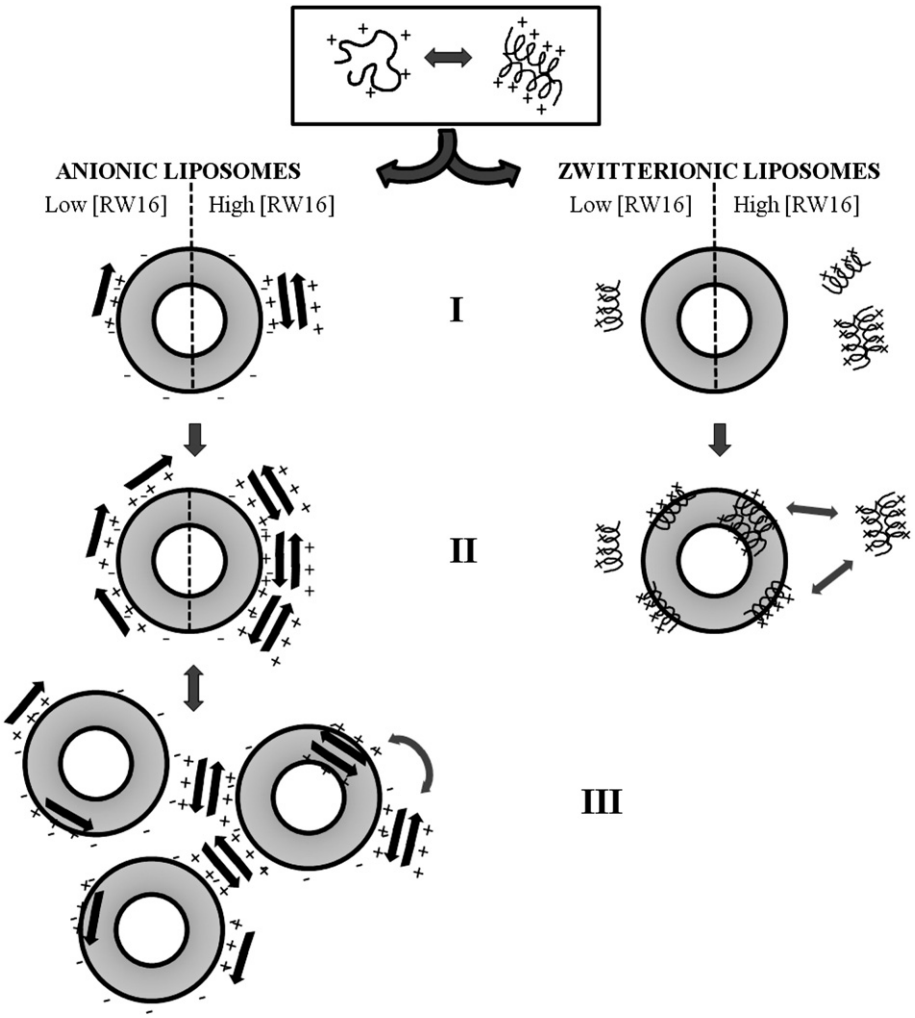

Fig. 9. Model proposed for the interaction of RW16 with zwitterionic vs anionic lipid model systems (left vs right panels) and for the peptide in its monomeric (low concentration, left part of the liposome) and oligomeric (high concentration, right part of the liposome) forms taking into consideration all experiments presented in this study. Discussion on the model can be found in the Conclusions section.

the oligomeric form (Fig. 9, top). The oligomerization leads to helical structure formation. The state of the peptide drastically changes its lipid interaction: in the monomer state the peptide can have both hydrophilic and hydrophobic areas exposed to solvent and so available for lipid interactions; in the oligomer state the peptide will mostly present its hydrophilic face (hydrophobic face will be mostly buried in the oligomer peptide core). This explains the disparity in the P/L affinity measured by PWR vs ITC experiments. Therefore, while at low nanomolar concentrations the peptide stays as a "monomer" and binds to the anionic membrane with rather strong affinity (~2 nM, PWR data), at micromolar concentrations the peptide is aggregated and binds with a lower affinity to the bilayer (in the micromolar range, ITC data) (Fig. 9, stage I, left panel). Binding of the peptide to anionic lipids would occur at first mainly by electrostatic interactions through the charged face of the peptide. This results in a non-favorable exposure of the hydrophobic face of the peptide. To deal with that the peptide either flips around the Arg residues to insert Trp residues in the membrane core or autoassociates to protect the hydrophobic face from the solvent. Peptide autoassociation leads to liposome aggregation (stages II and III, left panel in Fig. 9). Liposome aggregation can also result from the neutralization of the lipid surface charge by peptide binding, that decreases electrostatic repulsion leading to massive aggregation. The binding of the peptide to anionic lipids is accompanied by a conformation change to a β-sheet structure. In the presence of zwitterionic lipids, no binding was observed by ITC because the peptide is at high concentrations and so in the oligomer form, while in PWR an interaction is observed as the peptide is in the monomer form (Fig. 9, stage I, right panel). At increasing peptide concentrations, strong repulsions between the oligomers in solution may lead to the partial disruption of this oligomers and insertion in the membrane, the hydrophobic face of the peptide will be buried in the membrane (stage II, right panel, Fig. 9). The peptide remains α-helical. Overall, the experiments demonstrate that electrostatic interactions are important for the interaction and so enhanced interactions and perturbations of anionic lipids are observed relative to zwitterionic ones. This comes logically after what was found previously regarding cationic cell-penetrating peptide. Less expected is the fact that in the P/L interaction the hydrophobic interactions rather than electrostatic ones seem to predominate. So, if the electrostatic interactions (between the Arg in the peptide and the polar lipid headgroups) are important for a first fast membrane contact (Fig. 9, stage I), once this stage is passed the hydrophobic contacts (probably between the Trp residues and the fatty acid chain region, following peptide flip) become important (Fig. 9, stage II). Equilibrium between flipped and non-flipped peptide is proposed which in the case of non-flipped peptide leads to a peptide oligomerization to protect the peptide hydrophobic surface from the solvent (Fig. 9, stage III, left panel). Indeed calorimetry studies demonstrate the importance of hydrophobic contacts and fluorescent studies suggest that in both types of lipids the Trp residues change to a more hydrophobic environment, so inserted in the fatty acid chain region. A deeper insertion of the peptide in zwitterionic vs anionic lipids is suggested by DSC studies, probably resulting from the fact that in anionic lipids the peptide may be retained more at the surface due to the electrostatic interactions with the lipid headgroups (Fig. 9, stage I left panel vs right panel). The accumulation of peptide in the membrane, either in its monomeric or oligomeric form, will create a mass imbalance in the membrane that can lead to the formation of pores or defects in the membrane allowing peptide passage. This step, in the case of anionic lipids, is accompanied by stronger membrane perturbations with liposome oligomerization (Fig. 9, stage III, left panel) and the formation of other type of lipid supramolecular structures (as shown by Cryo-TEM). Aside from a preferential interaction with anionic lipids, RW16 would have the capacity of recruiting these lipids from binary lipid mixtures as shown by DSC. This is interesting when considering real cell membranes, for example from cancer cells that contain a few amounts of anionic lipids. When condensed in small domains these minor lipid components may present an increased potential. The enhanced interaction and perturbation observed in RW16 interaction with anionic lipids is interesting when considering the reported potential of this peptide in selectively affecting the motility and intracellular actin-remodeling activity of tumor cells [10]. Cancer cell membranes being particularly more anionic than those of healthy cells due to the presence of anionic lipids in their outer leaflet (PS mainly) and overexpression in certain proteoglycans (also rich in negative charges), such enhanced effect of RW16 on anionic membranes may explain its potential as possible anticancer agent. Indeed recent studies pointed to a selectivity of certain CPPs to cancer cells and tumors [12–14].

Supplementary data to this article can be found online at http://dx.doi.org/10.1016/j.bbamem.2013.02.008.

Acknowledgements

This work was supported by the French Ministère de l'Enseignement Supérieur et de la Recherche. We thank Rodrigue Marquant from the LBM, UMR 7613 (University Pierre et Marie Curie) for RW16 peptide synthesis and purification. We thank R. Oda from the CBMN, UMR 5248 (University of Bordeaux 1) and C. Schatz from the LCPO, UMR 5629 (University of Bordeaux 1) for DLS measurements. We thank O. Lambert from the CBMN, UMR 5248 (University of Bordeaux 1) for the use of the Cryo-TEM and fruitful discussions.

References

[1] M. Zorko, U. Langel, Cell-penetrating peptides: mechanism and kinetics of cargo delivery, Adv. Drug Deliv. Rev. 57 (2005) 529–545.
[2] G.P. Dietz, M. Bahr, Delivery of bioactive molecules into the cell: the Trojan horse approach, Mol. Cell. Neurosci. 27 (2004) 85–131.
[3] C. Foerg, H.P. Merkle, On the biomedical promise of cell penetrating peptides: limits versus prospects, J. Pharm. Sci. 97 (2008) 144–162.
[4] E. Gros, S. Deshayes, M.C. Morris, G. Aldrian-Herrada, J. Depollier, F. Heitz, G. Divita, A non-covalent peptide-based strategy for protein and peptide nucleic acid transduction, Biochim. Biophys. Acta 1758 (2006) 384–393.
[5] S. Moschos, A. Williams, M. Lindsay, In vivo applications of cell-penetrating peptide, in: U. Langel (Ed.), Cell-Penetrating Peptides, CRC Press, Boca Raton, 2007, pp. 423–438.
[6] L.N. Patel, J.L. Zaro, W.C. Shen, Cell penetrating peptides: intracellular pathways and pharmaceutical perspectives, Pharm. Res. 24 (2007) 1977–1992.
[7] A.T. Jones, E.J. Sayers, Cell entry of cell penetrating peptides: tales of tails wagging dogs, J. Control. Release 161 (2012) 582–591.
[8] H.A. Rydberg, M. Matson, H.L. Amand, E.K. Esbjorner, B. Norden, Effects of tryptophan content and backbone spacing on the uptake efficiency of cell-penetrating peptides, Biochemistry 51 (27) (2012) 5531–5539.
[9] D. Derossi, G. Chassaing, A. Prochiantz, Trojan peptides: the penetratin system for intracellular delivery, Trends Cell Biol. 8 (1998) 84–87.
[10] D. Delaroche, F.X. Cantrelle, F. Subra, C. Van Heijenoort, E. Guittet, C.Y. Jiao, L. Blanchoin, G. Chassaing, S. Lavielle, C. Auclair, S. Sagan, Cell-penetrating peptides with intracellular actin-remodeling activity in malignant fibroblasts, J. Biol. Chem. 285 (2010) 7712–7721.
[11] A. Lamaziere, F. Burlina, C. Wolf, G. Chassaing, G. Trugnan, J. Ayala-Sanmartin, Non-metabolic membrane tubulation and permeability induced by bioactive peptides, PLoS One 2 (2007) e201.
[12] S. Richter, V. Bouvet, M. Wuest, R. Bergmann, J. Steinbach, J. Pietzsch, I. Neundorf, F. Wuest, (18)F-Labeled phosphopeptide-cell-penetrating peptide dimers with enhanced cell uptake properties in human cancer cells, Nucl. Med. Biol. 39 (8) (2012) 1202–1212.
[13] I. Nakase, Y. Konishi, M. Ueda, H. Saji, S. Futaki, Accumulation of arginine-rich cell-penetrating peptides in tumors and the potential for anticancer drug delivery in vivo, J. Control. Release 159 (2012) 181–188.
[14] E. Kondo, K. Saito, Y. Tashiro, K. Kamide, S. Uno, T. Furuya, M. Mashita, K. Nakajima, T. Tsumuraya, N. Kobayashi, M. Nishibori, M. Tanimoto, M. Matsushita, Tumour lineage-homing cell-penetrating peptides as anticancer molecular delivery systems, Nat. Commun. 3 (2012) 951.
[15] J.H. Lee, H. Park, H. Chung, S. Choi, Y. Kim, H. Yoo, T.Y. Kim, H.J. Hann, I. Seong, J. Kim, K.G. Kang, I.O. Han, E.S. Oh, Syndecan-2 regulates the migratory potential of melanoma cells, J. Biol. Chem. 284 (2009) 27167–27175.
[16] K. Matsuda, H. Maruyama, F. Guo, J. Kleeff, J. Itakura, Y. Matsumoto, A.D. Lander, M. Korc, Glypican-1 is overexpressed in human breast cancer and modulates the mitogenic effects of multiple heparin-binding growth factors in breast cancer cells, Cancer Res. 61 (2001) 5562–5569.
[17] R.D. Sanderson, Heparan sulfate proteoglycans in invasion and metastasis, Semin. Cell Dev. Biol. 12 (2001) 89–98.
[18] I. Vlodavsky, O. Goldshmidt, E. Zcharia, R. Atzmon, Z. Rangini-Guatta, M. Elkin, T. Peretz, Y. Friedmann, Mammalian heparanase: involvement in cancer metastasis, angiogenesis and normal development, Semin. Cancer Biol. 12 (2002) 121–129.

[19] S.J. Martin, C.P. Reutelingsperger, A.J. McGahon, J.A. Rader, R.C. van Schie, D.M. LaFace, D.R. Green, Early redistribution of plasma membrane phosphatidylserine is a general feature of apoptosis regardless of the initiating stimulus: inhibition by overexpression of Bcl-2 and Abl, J. Exp. Med. 182 (1995) 1545–1556.
[20] S.T. Henriques, M.N. Melo, M.A. Castanho, Cell-penetrating peptides and antimicrobial peptides: how different are they? Biochem. J. 399 (2006) 1–7.
[21] I.D. Alves, N. Goasdoue, I. Correia, S. Aubry, C. Galanth, S. Sagan, S. Lavielle, G. Chassaing, Membrane interaction and perturbation mechanisms induced by two cationic cell penetrating peptides with distinct charge distribution, Biochim. Biophys. Acta 1780 (2008) 948–959.
[22] J.S. Bahnsen, H. Franzyk, A. Sandberg-Schaal, H.M. Nielsen, Antimicrobial and cell-penetrating properties of penetratin analogs: effect of sequence and secondary structure, Biochim. Biophys. Acta 1828 (2013) 223–232.
[23] C. Palm, S. Netzereab, M. Hallbrink, Quantitatively determined uptake of cell-penetrating peptides in non-mammalian cells with an evaluation of degradation and antimicrobial effects, Peptides 27 (2006) 1710–1716.
[24] K. Splith, I. Neundorf, Antimicrobial peptides with cell-penetrating peptide properties and vice versa, Eur. Biophys. J. 40 (2011) 387–397.
[25] P. Wadhwani, R.F. Epand, N. Heidenreich, J. Burck, A.S. Ulrich, R.M. Epand, Membrane-active peptides and the clustering of anionic lipids, Biophys. J. 103 (2012) 265–274.
[26] N. Papo, Y. Shai, New lytic peptides based on the D,L-amphipathic helix motif preferentially kill tumor cells compared to normal cells, Biochemistry 42 (2003) 9346–9354.
[27] S.A. Johnstone, K. Gelmon, L.D. Mayer, R.E. Hancock, M.B. Bally, In vitro characterization of the anticancer activity of membrane-active cationic peptides. I. Peptide-mediated cytotoxicity and peptide-enhanced cytotoxic activity of doxorubicin against wild-type and p-glycoprotein over-expressing tumor cell lines, Anticancer Drug Des. 15 (2000) 151–160.
[28] F.S. Kao, Y.R. Pan, R.Q. Hsu, H.M. Chen, Efficacy verification and microscopic observations of an anticancer peptide, CB1a, on single lung cancer cell, Biochim. Biophys. Acta 1818 (2012) 2927–2935.
[29] M. Amiche, A.A. Seon, H. Wroblewski, P. Nicolas, Isolation of dermatoxin from frog skin, an antibacterial peptide encoded by a novel member of the dermaseptin genes family, Eur. J. Biochem. 267 (2000) 4583–4592.
[30] P. Bonnafous, T. Stegmann, Membrane perturbation and fusion pore formation in influenza hemagglutinin-mediated membrane fusion. A new model for fusion, J. Biol. Chem. 275 (2000) 6160–6166.
[31] G. Rouser, S. Fkeischer, A. Yamamoto, Two dimensional then layer chromatographic separation of polar lipids and determination of phospholipids by phosphorus analysis of spots, Lipids 5 (1970) 494–496.
[32] T. Pott, E.J. Dufourc, Action of melittin on the DPPC-cholesterol liquid-ordered phase: a solid state 2H- and 31P-NMR study, Biophys. J. 68 (1995) 965–977.
[33] P. Mueller, D.O. Rudin, H.T. Tien, W.C. Wescott, Reconstitution of cell membrane structure in vitro and its transformation into an excitable system, Nature 194 (1962) 979–980.
[34] Z. Salamon, G. Tollin, I. Alves, V. Hruby, Chapter 6. Plasmon resonance methods in membrane protein biology applications to GPCR signaling, Methods Enzymol. 461 (2009) 123–146.
[35] I.D. Alves, S.M. Cowell, Z. Salamon, S. Devanathan, G. Tollin, V.J. Hruby, Different structural states of the proteolipid membrane are produced by ligand binding to the human delta-opioid receptor as shown by plasmon-waveguide resonance spectroscopy, Mol. Pharmacol. 65 (2004) 1248–1257.
[36] Z. Salamon, G. Tollin, Graphical analysis of mass and anisotropy changes observed by plasmon-waveguide resonance spectroscopy can provide useful insights into membrane protein function, Biophys. J. 86 (2004) 2508–2516.
[37] I.D. Alves, I. Correia, C.Y. Jiao, E. Sachon, S. Sagan, S. Lavielle, G. Tollin, G. Chassaing, The interaction of cell-penetrating peptides with lipid model systems and subsequent lipid reorganization: thermodynamic and structural characterization, J. Pept. Sci. 15 (2009) 200–209.
[38] S. Devanathan, Z. Salamon, G. Tollin, J. Fitch, T.E. Meyer, M.A. Cusanovich, Binding of oxidized and reduced cytochrome c2 to photosynthetic reaction centers: plasmon-waveguide resonance spectroscopy, Biochemistry 43 (2004) 16405–16415.
[39] P. Lecorche, A. Walrant, F. Burlina, L. Dutot, S. Sagan, J.M. Mallet, B. Desbat, G. Chassaing, I.D. Alves, S. Lavielle, Cellular uptake and biophysical properties of galactose and/or tryptophan containing cell-penetrating peptides, Biochim. Biophys. Acta 1818 (2012) 448–457.
[40] H. Binder, G. Lindblom, Charge-dependent translocation of the Trojan peptide penetratin across lipid membranes, Biophys. J. 85 (2003) 982–995.
[41] A. Ziegler, J. Seelig, Contributions of glycosaminoglycan binding and clustering to the biological uptake of the nonamphipathic cell-penetrating peptide WR9, Biochemistry 50 (2011) 4650–4664.
[42] A. Ziegler, J. Seelig, Binding and clustering of glycosaminoglycans: a common property of mono- and multivalent cell-penetrating compounds, Biophys. J. 94 (2008) 2142–2149.
[43] J.M. Seddon, Structure of the inverted hexagonal (HII) phase, and non-lamellar phase transitions of lipids, Biochim. Biophys. Acta 1031 (1990) 1–69.
[44] D.I. Chan, E.J. Prenner, H.J. Vogel, Tryptophan- and arginine-rich antimicrobial peptides: structures and mechanisms of action, Biochim. Biophys. Acta 1758 (2006) 1184–1202.
[45] D. Lichtenberg, E. Freire, C.F. Schmidt, Y. Barenholz, P.L. Felgner, T.E. Thompson, Effect of surface curvature on stability, thermodynamic behavior, and osmotic activity of dipalmitoylphosphatidylcholine single lamellar vesicles, Biochemistry 20 (1981) 3462–3467.
[46] S. Thennarasu, A. Tan, R. Penumatchu, C.E. Shelburne, D.L. Heyl, A. Ramamoorthy, Antimicrobial and membrane disrupting activities of a peptide derived from the human cathelicidin antimicrobial peptide LL37, Biophys. J. 98 (2010) 248–257.
[47] Y.P. Zhang, R.N. Lewis, R.S. Hodges, R.N. McElhaney, Interaction of a peptide model of a hydrophobic transmembrane alpha-helical segment of a membrane protein with phosphatidylcholine bilayers: differential scanning calorimetric and FTIR spectroscopic studies, Biochemistry 31 (1992) 11579–11588.
[48] R.F. Epand, M.A. Schmitt, S.H. Gellman, R.M. Epand, Role of membrane lipids in the mechanism of bacterial species selective toxicity by two alpha/beta-antimicrobial peptides, Biochim. Biophys. Acta 1758 (2006) 1343–1350.
[49] R.F. Epand, G. Wang, B. Berno, R.M. Epand, Lipid segregation explains selective toxicity of a series of fragments derived from the human cathelicidin LL-37, Antimicrob. Agents Chemother. 53 (2009) 3705–3714.
[50] R.M. Epand, R.F. Epand, C.J. Arnusch, B. Papahadjopoulos-Sternberg, G. Wang, Y. Shai, Lipid clustering by three homologous arginine-rich antimicrobial peptides is insensitive to amino acid arrangement and induced secondary structure, Biochim. Biophys. Acta 1798 (2010) 1272–1280.
[51] P. Joanne, C. Galanth, N. Goasdoue, P. Nicolas, S. Sagan, S. Lavielle, G. Chassaing, C. El Amri, I.D. Alves, Lipid reorganization induced by membrane-active peptides probed using differential scanning calorimetry, Biochim. Biophys. Acta 1788 (2009) 1772–1781.
[52] B.J. Potter, T.A. McHugh, O. Beloqui, Iron uptake from transferrin and asialotransferrin by hepatocytes from chronically alcohol-fed rats, Alcohol. Clin. Exp. Res. 16 (1992) 810–815.
[53] H. Leontiadou, A.E. Mark, S.J. Marrink, Antimicrobial peptides in action, J. Am. Chem. Soc. 128 (2006) 12156–12161.
[54] C.F. Lopez, S.O. Nielsen, G. Srinivas, W.F. Degrado, M.L. Klein, Probing membrane insertion activity of antimicrobial polymers via coarse-grain molecular dynamics, J. Chem. Theory Comput. 2 (2006) 649–655.
[55] L.E. Yandek, A. Pokorny, A. Floren, K. Knoelke, U. Langel, P.F. Almeida, Mechanism of the cell-penetrating peptide transportan 10 permeation of lipid bilayers, Biophys. J. 92 (2007) 2434–2444.
[56] D.K. Hincha, J.H. Crowe, The lytic activity of the bee venom peptide melittin is strongly reduced by the presence of negatively charged phospholipids or chloroplast galactolipids in the membranes of phosphatidylcholine large unilamellar vesicles, Biochim. Biophys. Acta 1284 (1996) 162–170.
[57] Z. Salamon, G. Tollin, Optical anisotropy in lipid bilayer membranes: coupled plasmon-waveguide resonance measurements of molecular orientation, polarizability, and shape, Biophys. J. 80 (2001) 1557–1567.
[58] W.T. Heller, A.J. Waring, R.I. Lehrer, T.A. Harroun, T.M. Weiss, L. Yang, H.W. Huang, Membrane thinning effect of the beta-sheet antimicrobial protegrin, Biochemistry 39 (2000) 139–145.
[59] A. Mecke, D.K. Lee, A. Ramamoorthy, B.G. Orr, M.M. Banaszak Holl, Membrane thinning due to antimicrobial peptide binding: an atomic force microscopy study of MSI-78 in lipid bilayers, Biophys. J. 89 (2005) 4043–4050.
[60] P. Garidel, A. Blume, Interaction of alkaline earth cations with the negatively charged phospholipid 1,2-dimyristoyl-sn-glycero-3-phosphoglycerol: a differential scanning and isothermal titration calorimetric study, Langmuir 15 (1999) 9.
[61] E. Barany-Wallje, S. Keller, S. Serowy, S. Geibel, P. Pohl, M. Bienert, M. Dathe, A critical reassessment of penetratin translocation across lipid membranes, Biophys. J. 89 (2005) 2513–2521.
[62] A. Walrant, A. Vogel, I. Correia, O. Lequin, B.E. Olausson, B. Desbat, S. Sagan, I.D. Alves, Membrane interactions of two arginine-rich peptides with different cell internalization capacities, Biochim. Biophys. Acta 1818 (2012) 1755–1763.
[63] M. Magzoub, L.E. Eriksson, A. Graslund, Conformational states of the cell-penetrating peptide penetratin when interacting with phospholipid vesicles: effects of surface charge and peptide concentration, Biochim. Biophys. Acta 1563 (2002) 53–63.
[64] R.W. Woody, Contributions of tryptophan side chains to the far-ultraviolet circular dichroism of proteins, Eur. Biophys. J. 23 (1994) 253–262.
[65] A.S. Ladokhin, M.E. Selsted, S.H. White, CD spectra of indolicidin antimicrobial peptides suggest turns, not polyproline helix, Biochemistry 38 (1999) 12313–12319.
[66] V.V. Andrushchenko, H.J. Vogel, E.J. Prenner, Solvent-dependent structure of two tryptophan-rich antimicrobial peptides and their analogs studied by FTIR and CD spectroscopy, Biochim. Biophys. Acta 1758 (2006) 1596–1608.
[67] A. Lamaziere, C. Wolf, O. Lambert, G. Chassaing, G. Trugnan, J. Ayala-Sanmartin, The homeodomain derived peptide penetratin induces curvature of fluid membrane domains, PLoS One 3 (2008) e1938.
[68] A. Lamaziere, O. Maniti, C. Wolf, O. Lambert, G. Chassaing, G. Trugnan, J. Ayala-Sanmartin, Lipid domain separation, bilayer thickening and pearling induced by the cell penetrating peptide penetratin, Biochim. Biophys. Acta 1798 (2010) 2223–2230.